

## Abstract

The socioeconomic losses from the recent unpreceded incidents in the electric power systems suggest the need for alternative planning strategies that account for the expected and extreme events that are less likely to occur. Such high impact low probability (HILP), or black swan, events are typically weather-related, have accounted for billions of dollars in economic losses, and left customers in the dark for several days. Furthermore, the proliferation of distributed energy resources (DERs) on the distribution grid indicates that system operators can also plan resilience from the customer's end, forming intentional microgrid islands when needed. However, existing planning strategies only minimize the expected operating cost and do not explicitly include the risk of extreme events. With the increasing frequency of black swan events in the current scenario, system operators should focus on the HILP events and find the optimal trade-off decision to maximize resilience with available resources. This proposal aims to investigate the impact of extreme weather events, hurricanes, and floods, on the power grid and propose planning solutions to enhance the grid's resilience. Firstly, we propose a modeling framework to assess the spatiotemporal compounding effect of hurricanes and storm surges on electric power systems. The spatiotemporal probabilistic loss metric helps system operators identify the potential impact and vulnerable components as the storm approaches. Secondly, we develop a risk-averse two-stage stochastic optimization framework for resilience planning of power distribution systems against extreme weather events. The resource planning strategy involves minimizing a risk metric, conditional value-at-risk (CVaR) while adhering to budget constraints for planning. The main idea is to identify a trade-off between risk-averse and risk-neutral planning solutions to maximize the energization of critical loads when a HILP event is realized. The problem is also extended to determine the trade-off among different resources when system operators have a limited budget. This facilitates the selection of specific resources from a portfolio of various resources that can optimally restore critical loads during the realization of a HILP event. In the future, the work will be extended to a larger and broader landscape with an analysis based on realistic extreme weather events and their impact on the power system. The goal will be to create a generic simulation platform capable of generating and assessing the impact of such events on the electric power grid. The work will also include large-scale integrated operational solutions to enhance the resilience of future power grids. Furthermore, advanced parallel algorithms based on dual decomposition methods will be explored for scalable implementation of stochastic programming problems.

# Contents

<b>1 Motivation</b>	<b>5</b>
<b>2 Objectives and Task Lists</b>	<b>7</b>
<b>3 MPOPF Modelling Tradeoffs: Linear vs Nonlinear Formulations</b>	<b>8</b>
3.1 Introduction and Motivation . . . . .	8
3.2 Problem Formulation: BFM-NL vs LinDistFlow . . . . .	9
3.2.1 Notations . . . . .	9
3.2.2 Objective Function . . . . .	10
3.2.3 Constraints: Side-by-Side Comparison . . . . .	11
3.3 Test Systems and Simulation Setup . . . . .	13
3.3.1 Test Systems . . . . .	13
3.3.2 Input Forecast Curves . . . . .	14
3.3.3 Simulation Workflow . . . . .	14
3.4 Results and Performance Analysis . . . . .	15
3.4.1 ADS10 Results . . . . .	17
3.4.2 IEEE123A Results . . . . .	18
3.4.3 IEEE123B Results . . . . .	19
3.5 Discussion: Key Insights for Decomposition Algorithms . . . . .	19
3.5.1 Computational Speedup . . . . .	19
3.5.2 Optimality Gap: The Core Tradeoff . . . . .	20
3.5.3 Reactive Power Control: A Critical Discrepancy . . . . .	21
3.5.4 Voltage and Power Feasibility . . . . .	22
3.5.5 Complementary Modeling Strategy: A Hybrid Approach . . . . .	23
3.6 Conclusions and Implications . . . . .	24
<b>4 Spatial Decomposition via Equivalent Network Approximation (ENApp)</b>	<b>26</b>
4.1 Introduction and Motivation . . . . .	26
4.2 Problem Formulation . . . . .	28
4.2.1 Notations . . . . .	28
4.2.2 MPCOPF with Batteries . . . . .	29
4.2.3 ENApp-based MPDOPF with Batteries . . . . .	30
4.3 Case Study Demonstration: IEEE 123 Bus Test System . . . . .	31
4.3.1 Test System Description . . . . .	31
4.3.2 Simulation Workflow . . . . .	31
4.4 Simulation Results and Performance Analysis . . . . .	32
4.4.1 5-Hour Horizon Results . . . . .	32
4.4.2 10-Hour Horizon: Scalability Analysis . . . . .	35

4.5	Summary and Discussion . . . . .	37
4.5.1	Key Observations . . . . .	39
4.5.2	Implementation Status and Future Work . . . . .	40
<b>5</b>	<b>Temporal Decomposition via Temporal Alternating Direction Method of Multipliers (tADMM)</b>	<b>42</b>
5.1	Introduction and Motivation . . . . .	42
5.2	LinDistFlow MPOPF with tADMM . . . . .	43
5.2.1	Problem Overview . . . . .	43
5.2.2	Variable Color Coding . . . . .	43
5.2.3	Sets and Indices . . . . .	43
5.2.4	tADMM Algorithm Structure . . . . .	44
5.2.5	Convergence Criteria . . . . .	46
5.3	Copper Plate MPOPF with tADMM (Simplified Case) . . . . .	47
5.3.1	Problem Overview . . . . .	47
5.3.2	Variable Color Coding . . . . .	47
5.3.3	tADMM Algorithm Structure . . . . .	47
5.4	Numerical Results . . . . .	50
5.4.1	Battery Actions and Convergence Analysis . . . . .	50
5.5	Convergence Criteria . . . . .	51
5.5.1	Convergence Criteria . . . . .	51
5.6	Algorithm Parameters . . . . .	52
5.6.1	Objective Function Components . . . . .	52
5.6.2	Algorithmic Parameters . . . . .	53
5.7	Appendix: Full Variable and Parameter Definitions . . . . .	53
5.7.1	System Bases . . . . .	53
5.7.2	SOC Bound Definitions . . . . .	53
5.7.3	Physical Interpretation . . . . .	53
5.8	Summary and Discussion . . . . .	54
5.8.1	Implementation Status . . . . .	54
<b>6</b>	<b>Future Works</b>	<b>57</b>
6.1	Task 1: Temporal Decomposition for Medium Sized Balanced Three-Phase Systems . . . . .	57
6.2	Task 2: Temporal Decomposition for Large Sized Unbalanced Three-Phase Systems . . . . .	57
6.3	Task 3: Concluding Research and Dissertation . . . . .	58
6.4	Timeline . . . . .	59

<b>7</b>	<b>Biography</b>	<b>60</b>
7.1	Publications . . . . .	60
7.2	Program of Study Course Work . . . . .	61
<b>Appendix</b>		<b>62</b>
.1	Full MPOPF Formulation with LinDistFlow . . . . .	62

# 1 Motivation

Optimal power flow (OPF) methods have become vital for efficiently managing distributed energy resources (DERs) such as photovoltaic (PV) and battery energy storage systems (BESS) at the grid edge, aiming to enhance system-level objectives including reliability, resilience, and cost-effectiveness [1, 2]. BESS, by mitigating the fluctuations of intermittent DERs, transforms the OPF problem from a classic single-period formulation into a multi-period, time-coupled optimization that demands intricate modeling and advanced computational methods [1, 3].

Centralized OPF (COPF) approaches typically rely on non-convex formulations—often based on the nonlinear branch flow model [4]—to coordinate controllable devices. Although such methods can provide accurate solutions for small networks [1, 3, 5], computational time and scalability issues limit their utility in large-scale, real-world systems. Metaheuristic and evolutionary algorithms [6] offer alternative solutions but generally struggle with local optimality and slow convergence, especially for high-dimensional multi-period OPF tasks.

To improve tractability, convex relaxations and linear approximations such as LinDistFlow [7] have been widely employed [1, 3, 7]. These methods deliver fast convergence but introduce non-negligible optimality gaps, particularly as network size and DER/BESS penetration increase, which has not been fully quantified in existing research [1]. Recent studies have highlighted this gap, advocating for a systematic comparison of non-convex and linearized frameworks across varied network conditions [1, 7].

Recognizing the limitations of centralized and linear-programming-based solutions, recent research—including our own—has focused on spatial and temporal decomposition for scalable multi-period OPF. Our group adapted the Equivalent Network Approximation (ENApp) framework to enable distributed MPOPF (MPDOPF) in battery-integrated networks, leveraging spatial partitioning to allow parallel solution of local OPF subproblems and reduce global computational burdens [8]. This approach harnesses the radial structure of distribution networks and significantly accelerates convergence while maintaining solution fidelity. Moreover, our models introduce a battery loss term exclusively in the objective function, preventing simultaneous charge/discharge operations and preserving problem convexity without integer variables [8].

Extensive validation against industry-standard IEEE test systems demonstrates that our ENApp-based distributed MPOPF delivers superior scalability and optimality compared with conventional centralized frameworks. These studies also provide a robust, side-by-side comparison of LinDistFlow and branch flow-based nonlinear models for MPOPF across real

distribution network scenarios [1].

Major remaining research gaps include the scalability and real-time applicability of centralized MPOPF approaches [3, 5, 9–11], and the slow convergence and master controller dependencies in existing distributed frameworks such as Benders decomposition [12]. The contribution of this work is the development and benchmarking of a spatially distributed multi-period OPF algorithm, overcoming these challenges and enabling practical, accurate, large-scale coordinated grid-edge resource management.

## 2 Objectives and Task Lists

The overarching goal of this work is to develop a computationally scalable framework for solving the Multi-Period Optimal Power Flow (MPOPF) problem in active distribution systems. The proposed framework aims to address the inherent complexity and non-convexity of MPOPF formulations – arising from temporal coupling of decision variables and high-dimensional system models – by designing and implementing decomposition-based algorithms. The resulting framework is expected to enable tractable and near-optimal solutions for realistic time horizons and large distribution feeders, while preserving the physical fidelity of the underlying models. The following tasks have been completed or are currently being pursued toward achieving the objectives of this study:

1. **Literature Review on Multi-Period Optimal Power Flow:** A comprehensive review was conducted on existing formulations of the MPOPF problem for active distribution systems. This provided insights into modeling temporal dependencies, handling storage dynamics, and integrating distributed energy resources in multi-period settings.
2. **Study of Decomposition-Based Optimization Techniques:** A review of decomposition algorithms, including Bilevel optimization methods, ADMM, and Differential Dynamic Programming (DDP), was carried out to understand their suitability for large-scale and temporally coupled optimization problems. The study highlighted key convergence properties and trade-offs between spatial and temporal decompositions.
3. **Implementation of Spatial Decomposition for MPOPF:** A spatially decomposed MPOPF formulation was implemented and tested on benchmark distribution systems. The method demonstrated improved scalability compared to monolithic optimization, though it remained limited in addressing the temporal coupling present in long-horizon studies.
4. **Development and Evaluation of Differential Dynamic Programming (DDP):** The DDP algorithm was formulated and implemented for the MPOPF problem. While the approach yielded solutions close to those obtained from brute-force optimization, it exhibited oscillatory convergence behavior and lacked strong theoretical guarantees. Further research is required to enhance its stability and convergence properties.
5. **Implementation of Temporal ADMM for MPOPF:** A temporal Alternating Direction Method of Multipliers (ADMM) approach is being developed to address the

scalability challenges associated with increasing time horizons. Preliminary results on a copper-plate system show excellent convergence, and current efforts focus on extending the implementation to LinDistFlow-based distribution models.

6. **Validation and Scalability Testing:** The final phase will involve validating the proposed algorithms on a large-scale system like the 9500-node (three-phase) feeder. The goal is to demonstrate the framework's scalability for realistic horizons (e.g.,  $T = 96$  i.e. 1 day at 15-minute intervals) and its applicability to operational optimization in distribution grids.
7. **Exploratory Study on Multiple-Source Optimal Power Flow (MS-OPF):** As a future research direction, the framework will be extended to accommodate multi-source configurations, enabling coordinated optimization across multiple substations and zones in distribution networks.

## 3 MPOPF Modelling Tradeoffs: Linear vs Nonlinear Formulations

### 3.1 Introduction and Motivation

As discussed in the previous chapters, multi-period optimal power flow (MPOPF) problems are essential for managing grid edge devices (GEDs) such as battery energy storage systems (BESS) and photovoltaic (PV) systems in modern electricity distribution networks (EDNs). The subsequent chapters of this report will focus on spatial and temporal decomposition techniques to make MPOPF computationally tractable for large-scale systems. However, *before* attempting any decomposition strategy, a fundamental question arises: **What formulation should be used to model the underlying power flow equations?**

This chapter addresses this critical question by comparing two widely-used MPOPF formulations:

1. **Nonlinear Branch Flow Model (BFM-NL):** Based on the original branch flow equations [13], this formulation yields a non-convex programming (NCP) problem that captures network losses and voltage-current relationships accurately but suffers from slow convergence.

2. **Linear Programming (LinDistFlow):** Based on the LinDistFlow approximation [7], this formulation simplifies the power flow equations into a linear program (LP) that converges rapidly but introduces an optimality gap by neglecting certain nonlinear terms.

The choice between these formulations has profound implications for decomposition algorithms. A poor initial formulation can lead to:

- Sub-optimal solutions even if the decomposition converges correctly
- Physically infeasible control set-points when validated through AC power flow
- Misleading reactive power dispatch strategies
- Inaccurate predictions of critical quantities like substation power and line losses

**Research Gap:** While previous work has explored both NCP [5, 14, 15] and LP-based [16–20] OPF methods, no comprehensive study has investigated how EDN size and GED penetration levels systematically affect the optimality gap and feasibility of linear approximations compared to nonlinear formulations.

**Contribution:** This chapter provides a systematic comparison of BFM-NL and LinDistFlow formulations across three test systems of varying scales and GED penetrations. The analysis reveals when linear approximations are acceptable and when they introduce critical errors—insights that directly inform the decomposition strategies presented in subsequent chapters.

## 3.2 Problem Formulation: BFM-NL vs LinDistFlow

### 3.2.1 Notations

The distribution system is modeled as a tree (connected graph) with  $\mathcal{N}$  representing the set of all buses (indexed with  $i, j$ , and  $k$ ). A directed edge from bus  $i$  to  $j$  is represented by  $ij$  and the set of edges is  $\mathcal{L}$ . Line resistance and reactance are  $r_{ij}$  and  $x_{ij}$ , respectively. The study is conducted for a horizon of  $T$  time steps, each of interval length  $\Delta t$ , with  $\tau = \{1, 2, \dots, T\}$  representing the set of all time-steps. The set of buses with PVs is  $\mathcal{D}$  and with batteries is  $\mathcal{B}$ , where  $\mathcal{D}, \mathcal{B} \subseteq \mathcal{N}_{\mathcal{L}}$  and  $\mathcal{N}_{\mathcal{L}}$  denotes the set of all load buses.

Key variables include:

- $V_j^t$ : voltage magnitude at bus  $j$  at time  $t$ , with  $v_j^t = (V_j^t)^2$

- $I_{ij}^t$ : current magnitude through line  $ij$  at time  $t$ , with  $l_{ij}^t = (I_{ij}^t)^2$
- $P_{ij}^t, Q_{ij}^t$ : real and reactive power flow through line  $ij$  at time  $t$
- $p_{L_j}^t, q_{L_j}^t$ : real and reactive load demand at bus  $j$  at time  $t$
- $p_{D_j}^t, q_{D_j}^t$ : real and reactive power from PV inverter at bus  $j$  at time  $t$
- $P_{c_j}^t, P_{d_j}^t$ : battery charging and discharging power at bus  $j$  at time  $t$
- $q_{B_j}^t$ : reactive power support from battery inverter at bus  $j$  at time  $t$
- $B_j^t$ : battery energy level at bus  $j$  at time  $t$
- $P_{Subs}^t$ : real power from substation at time  $t$
- $C^t$ : cost per kWh of substation power at time  $t$

Inverter and battery parameters:

- $S_{D_{R_j}}, S_{B_{R_j}}$ : apparent power capacity of PV and battery inverters
- $P_{B_{R_j}}, B_{R_j}$ : rated power and energy capacity of battery
- $\eta_c, \eta_d$ : charging and discharging efficiencies
- $soc_{min}, soc_{max}$ : safe state-of-charge limits (fractional)

### 3.2.2 Objective Function

The MPOPF objective is to minimize the total cost of substation power over the horizon, with a secondary penalty to prevent simultaneous charging and discharging (SCD) of batteries [21]:

$$\min \sum_{t=1}^T \{f_0^t + f_{SCD}^t\} \quad (1)$$

where

Table 1: Constraint comparison: BFM-NL vs LinDistFlow

Constraint Type	BFM-NL	LinDistFlow
Real power balance	Includes $r_{ij}l_{ij}^t$ loss	Neglects loss
Reactive power balance	Includes $x_{ij}l_{ij}^t$ loss	Neglects loss
Voltage drop (KVL)	Includes $(r_{ij}^2 + x_{ij}^2)l_{ij}^t$	Neglects term
Apparent power	Quadratic: $(P_{ij}^t)^2 + (Q_{ij}^t)^2 = l_{ij}^t v_i^t$	Not modeled
Battery reactive power	Quadratic: $(P_{B_j}^t)^2 + (q_{B_j}^t)^2 \leq S_{B_{R,j}}^2$	Hexagonal approx.

$$f_0^t = C^t P_{Subs}^t \Delta t$$

$$f_{SCD}^t = \alpha \sum_{j \in \mathcal{B}} \left\{ (1 - \eta_c) P_{c_j}^t + \left( \frac{1}{\eta_d} - 1 \right) P_{d_j}^t \right\}$$

The hyperparameter  $\alpha$  is tuned to ensure SCD is avoided for the given system configuration.

### 3.2.3 Constraints: Side-by-Side Comparison

The key difference between BFM-NL and LinDistFlow lies in the power flow equations. Table 1 provides a side-by-side comparison of the main constraints.

#### 3.2.3.1 Power Balance Equations: Real Power (BFM-NL):

$$\sum_{(j,k) \in \mathcal{L}} P_{jk}^t - (P_{ij}^t - r_{ij}l_{ij}^t) = p_j^t \quad (2)$$

#### Real Power (LinDistFlow):

$$\sum_{(j,k) \in \mathcal{L}} P_{jk}^t - P_{ij}^t = p_j^t \quad (3)$$

where  $p_j^t = (P_{d_j}^t - P_{c_j}^t) + p_{D_j}^t - p_{L_j}^t$

#### Reactive Power (BFM-NL):

$$\sum_{(j,k) \in \mathcal{L}} Q_{jk}^t - (Q_{ij}^t - x_{ij}l_{ij}^t) = q_j^t \quad (4)$$

**Reactive Power (LinDistFlow):**

$$\sum_{(j,k) \in \mathcal{L}} Q_{jk}^t - Q_{ij}^t = q_j^t \quad (5)$$

where  $q_j^t = q_{D_j}^t + q_{B_j}^t - q_{L_j}^t$

**3.2.3.2 Voltage Drop (KVL): BFM-NL:**

$$v_j^t = v_i^t - 2(r_{ij}P_{ij}^t + x_{ij}Q_{ij}^t) + (r_{ij}^2 + x_{ij}^2)l_{ij}^t \quad (6)$$

**LinDistFlow:**

$$v_j^t = v_i^t - 2(r_{ij}P_{ij}^t + x_{ij}Q_{ij}^t) \quad (7)$$

**3.2.3.3 Apparent Power and Current (BFM-NL only):**

$$(P_{ij}^t)^2 + (Q_{ij}^t)^2 = l_{ij}^t v_i^t \quad (8)$$

**3.2.3.4 Common Constraints:** The following constraints are identical for both formulations:

$$P_{Subs}^t \geq 0 \quad (9)$$

$$v_j^t \in [V_{min}^2, V_{max}^2] \quad (10)$$

$$q_{D_j}^t \in [-q_{D_{Max,j}}^t, q_{D_{Max,j}}^t], \quad q_{D_{Max,j}}^t = \sqrt{{S_{D_{R,j}}}^2 - {p_{D_j}^t}^2} \quad (11)$$

$$B_j^t = B_j^{t-1} + \Delta t (\eta_c P_{c_j}^t - \frac{1}{\eta_d} P_{d_j}^t) \quad (12)$$

$$P_{c_j}^t, P_{d_j}^t \in [0, P_{B_{R,j}}] \quad (13)$$

$$B_j^t \in [soc_{min} B_{R,j}, soc_{max} B_{R,j}] \quad (14)$$

**3.2.3.5 Battery Inverter Reactive Power: BFM-NL (Quadratic):**

$$(P_{B_j}^t)^2 + (q_{B_j}^t)^2 \leq S_{B_{R,j}}^2, \quad P_{B_j}^t = P_{d_j}^t - P_{c_j}^t \quad (15)$$

Table 2: Test system configurations

Parameter	ADS10	IEEE123A	IEEE123B
$n$	10	128	128
$n_L$	8	85	85
$n_D$	2	17	26
$n_B$	2	34	43
$p_{D_{R,j}}$	$0.33 p_{L_{R,j}}$	$0.33 p_{L_{R,j}}$	$1.00 p_{L_{R,j}}$
$p_{B_{R,j}}$	$0.33 p_{L_{R,j}}$	$0.33 p_{L_{R,j}}$	$1.00 p_{L_{R,j}}$
$\alpha$	12.62	8.994	2.124

**LinDistFlow (Hexagonal Approximation [22]):**

$$q_{B_j}^t \in [-\sqrt{3}(P_{B_j}^t + S_{B_{R,j}}), -\sqrt{3}(P_{B_j}^t - S_{B_{R,j}})] \quad (16a)$$

$$q_{B_j}^t \in [-\frac{\sqrt{3}}{2}S_{B_{R,j}}, \frac{\sqrt{3}}{2}S_{B_{R,j}}] \quad (16b)$$

$$q_{B_j}^t \in [\sqrt{3}(P_{B_j}^t - S_{B_{R,j}}), \sqrt{3}(P_{B_j}^t + S_{B_{R,j}})] \quad (16c)$$

### 3.3 Test Systems and Simulation Setup

#### 3.3.1 Test Systems

Three test systems of varying scales and GED penetrations were evaluated:

1. **ADS10:** A small 10-bus Active Distribution System (Figure 1) with 25% PV and 25% battery penetration. Each GED’s active power rating is 33% of the rated load power at the respective bus.
2. **IEEE123A:** The IEEE 123-bus test system (Figure 2) with moderate GED penetration—20% of load buses have PVs and 30% have batteries. Each GED’s active power rating is 33% of the rated load power.
3. **IEEE123B:** The IEEE 123-bus system with high GED penetration—30% of load buses have PVs and 50% have batteries. Each GED’s active power rating is 100% of the rated load power.

Table 2 summarizes the configurations, where  $n, n_L, n_D, n_B$  are the cardinalities of sets  $\mathcal{N}, \mathcal{N}_L, \mathcal{D}, \mathcal{B}$  respectively, and  $\alpha$  is the SCD penalty hyperparameter from eq. (1).

Common parameter values across all systems are given in Table 3.

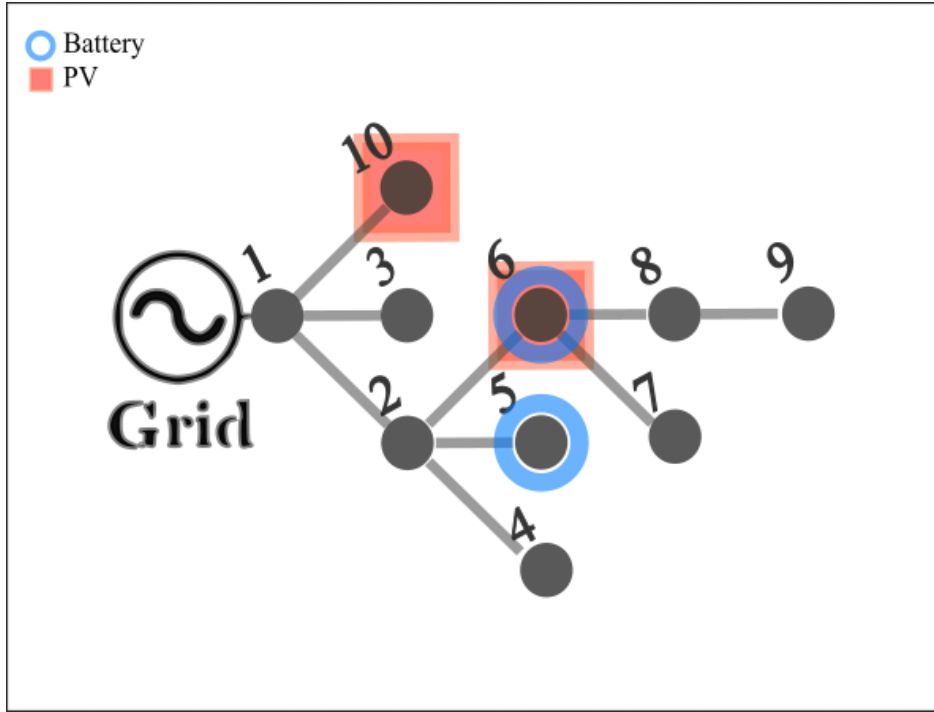


Figure 1: ADS10 test system with 25% PV and 25% BESS penetration

### 3.3.2 Input Forecast Curves

All systems use the same 24-hour forecast curves for load demand, PV irradiance, and time-varying electricity costs, as shown in Figure 3. The bilevel cost structure represents typical day-ahead pricing with peak and off-peak periods.

### 3.3.3 Simulation Workflow

The optimization problems were modeled in Julia using the JuMP package [23] and solved with the Ipopt solver [24]. Validation was performed using OpenDSS via the OpenDSSDirect.jl package [25].

For each test system:

1. Parse system topology and GED configuration from ‘.dss’ files
2. Apply common forecast curves from Figure 3
3. Convert to JuMP models representing 24-hour day-ahead planning

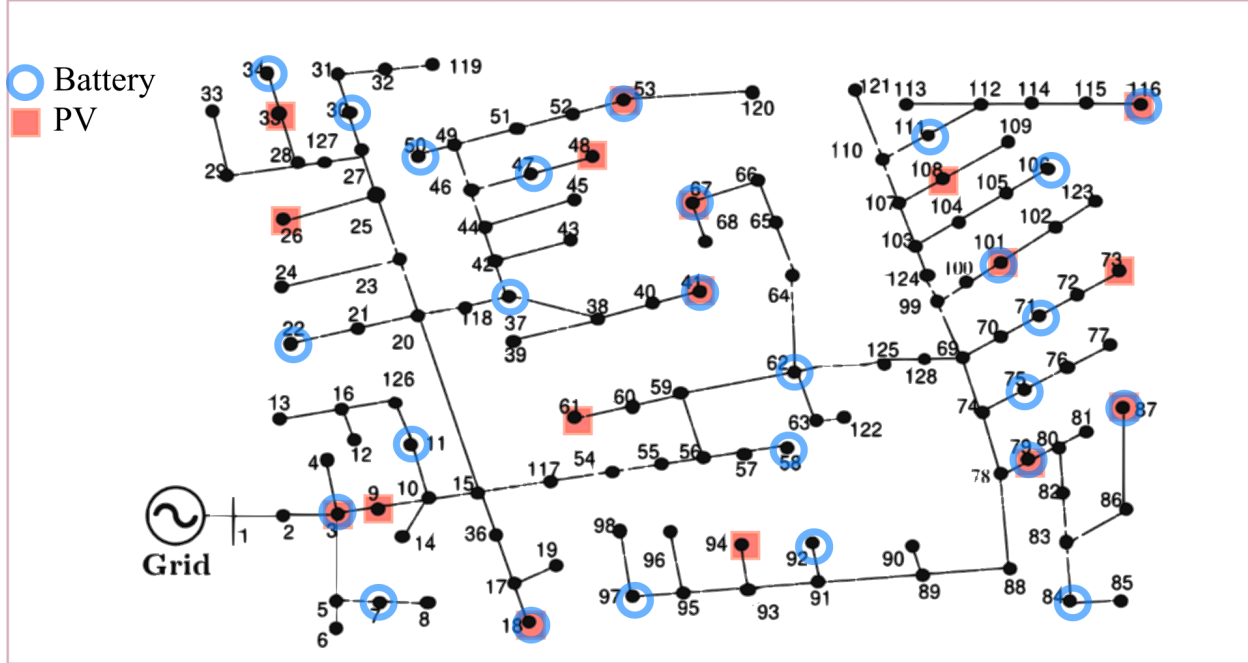


Figure 2: IEEE-123 test system with 20% PV and 30% BESS penetration (IEEE123A configuration)

4. Solve with Ipopt to obtain optimal control variables:  $P_{c_j}^t, P_{d_j}^t, q_{B_j}^t \forall j \in \mathcal{B}$  and  $q_{D_j}^t \forall j \in \mathcal{D}, \forall t \in \tau$
5. Feed control set-points into OpenDSS (preconfigured with same ‘.dss’ files)
6. Compare OpenDSS results (state and output variables) against optimization results to check for infeasibilities

**Important Note:** For LinDistFlow, the reported results use OpenDSS outputs when fed with LinDistFlow control variables. This is because LinDistFlow, by design, does not account for network losses, leading to underestimated values of  $P_{Subs}^t$  and line losses. This conjunction is denoted by LinDistFlow<sup>®</sup> in the results tables. The complete code is available in [26].

### 3.4 Results and Performance Analysis

Results are presented in two sets of tables per test system:

Table 3: Common parameter values

Parameter	Value
$V_{min}, V_{max}$	0.95 pu, 1.05 pu
$S_{D_{R,j}}$	$1.2 p_{D_{R,j}}$
$S_{B_{R,j}}$	$1.2 P_{B_{R,j}}$
$B_{R,j}$	$T_{fullCharge} \times P_{B_{R,j}}$
$T_{fullCharge}$	4 h
$T$	24
$\Delta t$	1 h
$\eta_c, \eta_d$	0.95, 0.95
$soc_{min}, soc_{max}$	0.30, 0.95

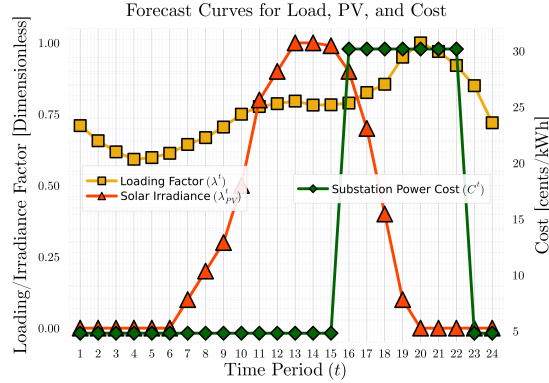


Figure 3: Forecasts for demand power, irradiance, and cost of substation power over a 24-hour horizon

1. **Optimality Tables** (Tables 4, 6 and 8): Direct performance comparison highlighting optimization metrics (substation cost, power, losses, computation time)
2. **Feasibility Tables** (Tables 5, 7 and 9): Validation via OpenDSS quantifying discrepancies in state/output variables

### 3.4.1 ADS10 Results

Table 4: MPOPF performance comparison - ADS10 test system for 24h

Metric	BFM-NL	LinDistFlow <sup>①</sup>
<i>Full horizon</i>		
Substation power cost (\$)	204.27	204.28
Substation real power (kWh)	1528.35	1528.4
Line loss (kWh)	0.28	0.33
Substation reactive power (kVARh)	428.9	795.56
PV reactive power (kVARh)	174.41	-0.69
Battery reactive power (kVARh)	192.8	-0.37
<i>Computation</i>		
Total simulation time (s)	2.64	0.77

Table 5: MPOPF discrepancy comparison - ADS10 test system for 24h

Metric	BFM-NL	LinDistFlow
<i>Max. all-time discrepancy</i>		
Voltage (pu)	0.00001	0.00001
Line loss (kW)	0.000009	0.000006
Substation power (kW)	0.000014	0.02410
Substation reactive power (kVAR)	0.070706	0.05618

### 3.4.2 IEEE123A Results

Table 6: MPOPF performance comparison - IEEE123-A test system for 24h

Metric	BFM-NL	LinDistFlow <sup>®</sup>
<i>Model dimensions</i>		
Decision variables	15144	12096
Linear constraints	18456	22200
Nonlinear constraints	3672	0
<i>Simulation results</i>		
Substation power cost (\$)	2787.44	2798.4
Substation real power (kWh)	20984.89	21065.89
Line loss (kWh)	380.09	461.38
Substation reactive power (kVARh)	6835.82	12259.29
PV reactive power (kVARh)	1972.27	195.12
Battery reactive power (kVARh)	3709.71	204.63
<i>Computation</i>		
Total simulation time (s)	17.44	0.85

Table 7: MPOPF discrepancy comparison - IEEE123-A test system for 24h

Metric	BFM-NL	LinDistFlow
<i>Max. all-time discrepancy</i>		
Voltage (pu)	0.00007	0.00206
Line loss (kW)	0.01818	1.8074
Substation power (kW)	0.43164	32.362
Substation reactive power (kVAR)	1.0102	64.403

### 3.4.3 IEEE123B Results

Table 8: MPOPF performance comparison - IEEE123-B test system for 24h

Metric	BFM-NL	LinDistFlow <sup>®</sup>
<i>Model dimensions</i>		
Decision variables	17184	14136
Linear constraints	24168	30360
Nonlinear constraints	4080	0
<i>Simulation results</i>		
Substation power cost (\$)	1973.83	1987.78
Substation real power (kWh)	16594.11	16693.01
Line loss (kWh)	234.78	333.78
Substation reactive power (kVARh)	-404.91	11055.41
PV reactive power (kVARh)	7255.22	1535.29
Battery reactive power (kVARh)	5371.97	-190.93
<i>Computation</i>		
Total simulation time (s)	23.75	1.66

Table 9: MPOPF discrepancy comparison - IEEE123-B test system for 24h

Metric	BFM-NL	LinDistFlow
<i>Max. all-time discrepancy</i>		
Voltage (pu)	0.000059	0.001599
Line loss (kW)	0.00776	1.055093
Substation power (kW)	0.217433	23.344019
Substation reactive power (kVAR)	1.016894	45.925288

## 3.5 Discussion: Key Insights for Decomposition Algorithms

This section synthesizes the simulation results to highlight critical insights that directly inform the choice of formulation for spatial and temporal decomposition algorithms presented in subsequent chapters.

### 3.5.1 Computational Speedup

As expected, the LinDistFlow model significantly outperforms BFM-NL in computation time, achieving speedups of approximately **3×**, **20×**, and **14×** for ADS10, IEEE123A, and

IEEE123B systems respectively. This performance gain stems primarily from the elimination of nonlinear constraints (tables 6 and 8 show zero nonlinear constraints for LinDistFlow).

Although LinDistFlow may include more total constraints (all linear) than BFM-NL's combination of linear and nonlinear ones, solve times remain dominated by the elimination of nonlinearity. Modern LP solvers handle large numbers of linear constraints efficiently, whereas nonlinear solvers must iteratively navigate non-convex landscapes.

**Note:** All BFM-NL timings assume a cold start. Warm-starting BFM-NL with LinDistFlow solutions would likely narrow the computational gap further—a strategy worth considering for decomposition algorithms where subproblems are solved repeatedly.

### 3.5.2 Optimality Gap: The Core Tradeoff

Since the objective function is the cost of total substation power borrowed over the horizon ( $f_0 = \sum_{t=1}^T C^t P_{Subs}^t \Delta t$  from eq. (1)), we quantify the optimality gap as:

$$\text{Optimality Gap} = \frac{f_{\text{LinDistFlow}} - f_{\text{BFM-NL}}}{f_{\text{BFM-NL}}} \times 100\%$$

Computing from tables 4, 6 and 8:

- **ADS10:** Gap = 0.005% (essentially negligible)
- **IEEE123A:** Gap = 0.39% (acceptable for many applications)
- **IEEE123B:** Gap = 0.71% (caution required)

**Analysis:** The optimality gap grows with both system size and GED penetration. Two primary factors explain this trend:

1. **Line Loss Approximation:** Larger systems experience greater line losses. LinDistFlow neglects the  $(r_{ij}^2 + x_{ij}^2)l_{ij}^t$  term in the KVL equation (eq. (7) vs eq. (6)) and the loss terms in power balance equations (eqs. (3) and (5) vs eqs. (2) and (4)). As losses increase, this approximation error compounds.
2. **Battery Inverter Reactive Power Model:** Higher battery penetration amplifies errors from the hexagonal approximation (eq. (16)) compared to the true quadratic constraint (eq. (15)). This is especially pronounced in IEEE123B where battery ratings equal load ratings (100% penetration).

**Implication for Decomposition:** When developing spatial or temporal decomposition algorithms (Chapters ?? and ??), using LinDistFlow as the base formulation will propagate this optimality gap. For large-scale systems or high DER penetrations, this gap may be unacceptable. However, for moderate-sized systems with lower penetrations, the computational speedup may justify the small optimality sacrifice.

### 3.5.3 Reactive Power Control: A Critical Discrepancy

One of the most striking differences between the two formulations is their reactive power management strategy, as seen in the “PV reactive power” and “Battery reactive power” rows of tables 4, 6 and 8.

**BFM-NL Behavior:** Deliberately allocates reactive power among PV inverters, batteries, and the substation based on:

- Network losses (via the  $l_{ij}^t x_{ij}$  term in eq. (4))
- Device capabilities and locations
- Voltage sensitivity at each bus

For example, in IEEE123A (moderate GED penetration), BFM-NL assigns:

- 1972 kVARh to PV inverters
- 3710 kVARh to battery inverters
- 6836 kVARh from substation

**LinDistFlow Behavior:** By dropping the  $l_{ij}^t x_{ij}$  term (eq. (5)), LinDistFlow loses sensitivity to how reactive power dispatch affects line losses. Consequently, it assigns reactive power in an almost arbitrary manner—often defaulting most reactive support to the substation:

- 195 kVARh to PV inverters ( $10\times$  less than BFM-NL)
- 205 kVARh to battery inverters ( $18\times$  less than BFM-NL)
- 12259 kVARh from substation ( $1.8\times$  more than BFM-NL)

**Practical Consequences:**

- Under-utilization of Distributed Assets:** LinDistFlow fails to leverage the reactive power capability of distributed inverters, missing opportunities for localized voltage support and loss reduction.
- Substation Overload Risk:** Concentrating reactive power at the substation may violate transformer ratings or lead to inefficient operation.
- Voltage Profile Degradation:** While both models achieve similar substation costs, LinDistFlow's coarse reactive dispatch risks larger voltage deviations throughout the network, especially during contingencies.
- Missed Grid Support Opportunities:** Modern grid codes increasingly require DERs to provide reactive support. LinDistFlow-based control strategies would systematically under-utilize this capability.

**Implication for Decomposition:** If the objective function includes voltage regulation, reactive power costs, or inverter utilization penalties (beyond simple substation cost minimization), LinDistFlow-based decomposition algorithms will produce fundamentally flawed solutions. Even for cost-minimization objectives, the reactive power mismatch creates operational risks that may be unacceptable in practice.

### 3.5.4 Voltage and Power Feasibility

Tables 5, 7 and 9 quantify discrepancies when control set-points from each model are applied in OpenDSS. These are computed as:

$$\begin{aligned} \text{Disc}_v &= \max_{j \in \mathcal{N}, t \in \tau} |V_{j,\text{OpenDSS}}^t - V_{j,\text{model}}^t| \\ \text{Disc}_{P_{\text{Subs}}} &= \max_{t \in \tau} |P_{\text{Subs},\text{OpenDSS}}^t - P_{\text{Subs},\text{model}}^t| \end{aligned}$$

**Voltage Deviation:** LinDistFlow maintains voltage errors under **0.2%** compared to BFM-NL (which itself has negligible errors). For most distribution operations, this is acceptable and unlikely to cause voltage limit violations.

**Substation Power Underprediction:** This is the critical concern. LinDistFlow can under-predict hourly substation power by up to **2–5%** (24–32 kW for IEEE123A, which represents hundreds of kWh over the horizon). This creates three operational risks:

- Equipment Limit Violations:** If the actual substation draw approaches transformer ratings, LinDistFlow's underestimation may lead to overloads.

2. **Reserve Margin Errors:** System operators rely on accurate power predictions to maintain adequate reserves. A 5% error can compromise reliability during contingencies.
3. **Economic Inaccuracies:** In real-time markets, substation power ties directly to settlement costs. Systematic underprediction leads to unexpected charges and missed arbitrage opportunities.

**Implication for Decomposition:** When using LinDistFlow-based decomposition, the subproblem solutions will consistently underestimate substation power and line losses. Aggregating these errors across spatial regions or temporal windows can produce dangerously optimistic predictions. Post-processing corrections or warm-starting with LinDistFlow followed by BFM-NL refinement becomes essential.

### 3.5.5 Complementary Modeling Strategy: A Hybrid Approach

Based on the above analysis, a purely LinDistFlow-based or purely BFM-NL-based approach each has critical limitations:

**LinDistFlow Strengths:**

- Fast convergence ( $10\text{--}20\times$  speedup)
- Near-optimal cost objective (within 0.4–0.7% for moderate systems)
- Suitable for rapid scenario screening or initialization

**LinDistFlow Weaknesses:**

- Under-reports substation power and line losses
- Arbitrary reactive power allocation
- Optimality gap grows with system size and GED penetration

**BFM-NL Strengths:**

- Accurate physics representation
- Physically consistent control and state variables
- Intelligent reactive power dispatch

### **BFM-NL Weaknesses:**

- Slow convergence (especially for cold starts)
- May struggle with large-scale systems without decomposition

**3.5.5.1 Recommended Hybrid Strategy:** For the spatial and temporal decomposition algorithms developed in subsequent chapters, we recommend:

1. **Phase 1 (Initialization):** Solve the MPOPF problem using LinDistFlow to quickly obtain near-optimal control set-points. Use these to warm-start the subsequent phase.
2. **Phase 2 (Refinement):** Solve the MPOPF problem using BFM-NL, initialized with Phase 1 results. This captures accurate physics while benefiting from the warm start to reduce computation time.
3. **Phase 3 (Validation):** Always validate final control set-points through OpenDSS or another AC power flow solver before deployment.

This hybrid approach provides a **feasible and optimal solution suitable for real-time operations** while maintaining computational tractability. The spatial decomposition (ENApp) and temporal decomposition (ADMM) algorithms presented in the following chapters can incorporate either formulation or this hybrid strategy depending on the application requirements.

## **3.6 Conclusions and Implications**

This chapter has demonstrated that the choice of power flow formulation—before any decomposition is attempted—has profound implications for solution quality, computational efficiency, and operational feasibility. The key findings are:

1. **Optimality Gap:** LinDistFlow introduces a gap that grows from 0.005% (small systems) to 0.7% (large systems with high GED penetration). While acceptable for cost minimization in moderate-sized systems, this gap may be unacceptable for large-scale deployments.
2. **Reactive Power Mismanagement:** LinDistFlow systematically under-utilizes distributed inverter assets, concentrating reactive power at the substation. This creates operational risks and misses grid support opportunities.

3. **Substation Power Underprediction:** LinDistFlow can underestimate hourly substation power by up to 5%, risking equipment overloads, reserve margin violations, and economic inaccuracies.
4. **Computational Speedup:** LinDistFlow achieves 10–20× faster solve times by eliminating nonlinear constraints, making it attractive for rapid scenario analysis or warm-start initialization.

**Central Insight:** *The formulation you choose fundamentally shapes the behavior of any decomposition algorithm built on top of it.* A spatially or temporally decomposed MPOPF using LinDistFlow will inherit its reactive power mismanagement and substation power errors, even if the decomposition itself converges correctly. Conversely, a decomposed BFM-NL approach will be more computationally expensive but will produce physically consistent and operationally sound solutions.

**Forward Connection:** The subsequent chapters develop:

- **Chapter on Spatial Decomposition (ENApp):** A spatially distributed MPOPF algorithm that partitions the network into areas. The insights from this chapter inform whether to use BFM-NL, LinDistFlow, or a hybrid approach for the area subproblems.
- **Chapter on Temporal Decomposition (tADMM):** An ADMM-based temporal decomposition that breaks the multi-period problem into single-period subproblems. The formulation choice (BFM-NL vs LinDistFlow) directly affects convergence behavior and solution quality.

By carefully considering the tradeoffs analyzed in this chapter, the decomposition algorithms can be designed to balance computational efficiency with solution accuracy, ultimately enabling scalable and reliable MPOPF for modern distribution networks with high penetrations of grid edge devices.

## 4 Spatial Decomposition via Equivalent Network Approximation (ENApp)

### 4.1 Introduction and Motivation

Optimal power flow (OPF) methods are employed to optimally coordinate grid’s controllable resources for different system-level objectives, such as economic operations, reliability, and resilience. The significance of OPF studies is growing in relevance at the distribution system level, driven by the increasing adoption of distributed energy resources (DERs), particularly photovoltaic systems (PVs) and battery energy storage systems (BESS). Furthermore, the adoption of BESS is gaining significance for managing the variability of DERs through controlled charging and discharging, thereby ensuring supply-demand balance [27]. Incorporating BESS into OPF problems substantially raises the complexity of network optimization problems, transitioning from a single-period, time-decoupled OPF to a multi-period, time-coupled OPF.

Traditionally, centralized OPF (COPF) methods have been widely used, where a central controller processes aggregated grid-edge data, executes the OPF algorithm, and sends control signals to manage resources [18]. The COPF algorithms for DER management are generally developed as a mixed integer non-convex programming (MINCP) problem and then simplified either as a convex problem by adopting second-order cone programming (SOCP) relaxations [28] [29], or as a linear problem by adopting Taylor series expansion [18], polyhedral approximations [30] or linear power flow models [31]. Unfortunately, COPF methods pose scalability challenges for larger networks and for difficult classes of OPF problems such multi-period time-coupled formulations required to optimally manage BESS.

To address scalability challenges, distributed OPF (DOPF) algorithms have been introduced. These algorithms decompose the COPF problem into smaller sub-problems that are solved concurrently, leveraging communication among neighboring areas. In this context, the Auxiliary Problem Principle (APP) and the Alternating Direction Method of Multipliers (ADMM) are widely adopted algorithms for solving various OPF problems, including non-convex formulations [32], convex-relaxed versions [33–35], and linear approximations [36]. Similarly, in a prior study [37], the authors’ research group introduced a DOPF framework utilizing the Equivalent Network Approximation method (ENApp). This approach was shown to require fewer macro iterations compared to traditional ADMM or APP algorithms for solving DOPF problems.

The above references [28]- [36] mainly focused on solving single time-period OPF prob-

lems and did not include the coordination of grid-edge devices that introduce time-coupled constraints, such as BESS. The inclusion of BESS models results in a multi-period OPF (MPOPF) problem with time-coupled constraints. Reference [5] proposed a nonlinear multi-period centralized OPF (MPCOPF) approach to optimally coordinate active-reactive power dispatch from batteries and DERs in distribution systems. Alizadeh and Capitanescu [38] proposed a stochastic security-constrained MPCOPF, which sequentially solves a specific number of linear approximations of the original problem. Usman and Capitanescu [39] developed three different MPCOPF frameworks. All three approaches begin by solving a linear program to optimize the binary variables first, followed by either a linear or non-linear program to optimize the continuous variables. Optimal battery schedules are determined in [40] considering uncertain renewable power generation by solving an MPCOPF. A bi-level robust MPCOPF is suggested in [41] for determining active and reactive power dispatches from the grid edge devices. Wu et al. [12] framed a Benders Decomposition (BD) based multi-period distributed OPF (MPDOPF) after decomposing the original centralized multi-parametric quadratic problem into one master and multiple sub-problems.

Over recent years, numerous research efforts have focused on developing MPOPF methodologies. However, the following research gaps persist:

1. The MPOPF models are mainly solved centrally [5]- [41]. The centralized methods suffer from scalability and computational challenges, requiring significantly long solution times, rendering them unsuitable for operational decision-making.
2. Reference [12] proposed a MPDOPF framework using Benders Decomposition. However, this approach suffers from slow convergence and needs a central controller to solve the master problem.

This work aims to address the above research gaps by developing a spatially distributed MPOPF (MPDOPF) framework. The distribution system is divided into multiple connected areas, each solving its own local MPOPF problem and periodically communicating the values of boundary variables with neighboring areas. The interaction between the areas is modeled by following the principles of the ENApp DOPF algorithm. ENApp outperforms the other DOPF algorithms in terms of convergence speed and requires fewer macro iterations [37]. The specific contributions of this work are listed below:

1. A MPOPF framework is proposed for distribution systems consisting of DERs and batteries. The integer variables related to battery charging/discharging are avoided by

adding a “Battery Loss” cost term in the objective function. The loss term will ensure the non-occurrence of simultaneous charging/discharging operations.

2. The original MPOPF framework is solved in a distributed manner by following the principles of the ENApp-based distributed OPF. This provides faster convergence and requires less solution time compared to the traditional MPCOPF.
3. Detailed comparative analyses between traditional MPCOPF and the proposed MP-DOPF are done using the IEEE 123 bus test system and the benefits of the proposed approach are demonstrated. ACOPF feasibility validation is also performed by implementing the derived controls into an OpenDSS model of the test system.

## 4.2 Problem Formulation

### 4.2.1 Notations

In this study, the distribution system is modeled as a tree (connected graph) with  $N$  number of buses (indexed with  $i$ ,  $j$ , and  $k$ ); the study is conducted for  $T$  time steps (indexed by  $t$ ), each of interval length  $\Delta t$ . The sets of buses with DERs and batteries are  $D$  and  $B$  respectively, such that  $D, B \subseteq N$ . A directed edge from bus  $i$  to  $j$  in the tree is represented by  $ij$  and the set for edges is given by  $\mathcal{L}$ . Line resistance and reactance are  $r_{ij}$  and  $x_{ij}$ , respectively. Magnitude of the current flowing through the line at time  $t$  is denoted by  $I_{ij}^t$  and  $l_{ij}^t = (I_{ij}^t)^2$ . The voltage magnitude of bus  $j$  at time  $t$  is given by  $V_j^t$  and  $v_j^t = (V_j^t)^2$ . Apparent power demand at a node  $j$  at time  $t$  is  $s_{L_j}^t$  ( $= p_{L_j}^t + j q_{L_j}^t$ ). The active power generation from the DER present at bus  $j$  at time  $t$  is denoted by  $p_{D_j}^t$  and controlled reactive power dispatch from the DER inverter is  $q_{D_j}^t$ . DER inverter capacity is  $S_{D_{R_j}}$ . The apparent power flow through line  $ij$  at time  $t$  is  $S_{ij}^t$  ( $= P_{ij}^t + j Q_{ij}^t$ ). The real power flowing from the substation into the network is denoted by  $P_{Subs}^t$  and the associated cost involved per kWh is  $C^t$ . The battery energy level is  $B_j^t$ . Charging and discharging active power from battery inverter (of apparent power capacity  $S_{B_{R_j}}$ ) are denoted by  $P_{c_j}^t$  and  $P_{d_j}^t$ , respectively and their associated efficiencies are  $\eta_c$  and  $\eta_d$ , respectively. The energy capacity of the batteries is denoted by  $B_{R_j}$ , and the rated battery power is  $P_{B_{R_j}}$ .  $soc_{min}$  and  $soc_{max}$  are fractional values for denoting safe soc limits of a battery about its rated state-of-charge (soc) capacity. The reactive power support of the battery inverter is indicated by  $q_{B_j}^t$ .

### 4.2.2 MPCOPF with Batteries

The OPF problem aims to minimize two objectives as shown in eq. (17). The first term in eq. (17) aims to minimize the total energy cost for the entire horizon. Including the ‘Battery Loss’ cost as the second term ( $\alpha > 0$ ) helps eliminate the need for binary (integer) variables typically used to prevent simultaneous charging and discharging. The resulting OPF problem is a non-convex optimization problem [21].

$$\min \sum_{t=1}^T \left[ C^t P_{Subs}^t \Delta t + \alpha \sum_{j \in \mathcal{B}} \left\{ (1 - \eta_C) P_{C_j}^t + \left( \frac{1}{\eta_D} - 1 \right) P_{D_j}^t \right\} \right] \quad (17)$$

Subject to the constraints eqs. (18) to (28) as given below:

$$\begin{aligned} \sum_{(j,k) \in \mathcal{L}} \{P_{jk}^t\} - (P_{ij}^t - r_{ij} l_{ij}^t) &= (P_{d_j}^t - P_{c_j}^t) \\ &\quad + p_{D_j}^t - p_{L_j}^t \end{aligned} \quad (18)$$

$$\sum_{(j,k) \in \mathcal{L}} \{Q_{jk}^t\} - (Q_{ij}^t - x_{ij} l_{ij}^t) = q_{D_j}^t + q_{B_j}^t - q_{L_j}^t \quad (19)$$

$$v_j^t = v_i^t - 2(r_{ij} P_{ij}^t + x_{ij} Q_{ij}^t) + \{r_{ij}^2 + x_{ij}^2\} l_{ij}^t \quad (20)$$

$$(P_{ij}^t)^2 + (Q_{ij}^t)^2 = l_{ij}^t v_i^t \quad (21)$$

$$P_{Subs}^t \geq 0 \quad (22)$$

$$v_j^t \in [V_{min}^2, V_{max}^2] \quad (23)$$

$$q_{D_j}^t \in \left[ -\sqrt{{S_{D_{R,j}}}^2 - {p_{D_j}^t}^2}, \sqrt{{S_{D_{R,j}}}^2 - {p_{D_j}^t}^2} \right] \quad (24)$$

$$B_j^t = B_j^{t-1} + \Delta t \eta_c P_{c_j}^t - \Delta t \frac{1}{\eta_d} P_{d_j}^t \quad (25)$$

$$P_{c_j}^t, P_{d_j}^t \in [0, P_{B_{R_j}}], \quad B_j^0 = B_j^T \quad (26)$$

$$q_{B_j}^t \in [-\sqrt{0.44} P_{B_{R,j}}, \sqrt{0.44} P_{B_{R,j}}] \quad (27)$$

$$B_j^t \in [soc_{min} B_{R,j}, soc_{max} B_{R,j}] \quad (28)$$

A branch power flow model, given by eqs. (18) to (21), is used to represent power flow in distribution system. Constraints eqs. (18) and (19) model the active and reactive power balance at node  $j$ , respectively. The KVL equation for branch  $(ij)$  is represented by eq. (20), while the equation describing the relationship between current magnitude, voltage magnitude and apparent power magnitude for branch  $(ij)$  is given by eq. (21). Backflow of real power into the substation from the distribution system is avoided using the constraint eq. (22). The allowable limits for bus voltages are modeled via eq. (23). eq. (24) describes the reactive power limits of DER inverters. The trajectory of the battery energy versus time is given by eq. (25) (this is a time-coupled constraint). Battery charging and discharging powers are limited by the battery's rated power capacity, as given by eq. (26). eq. (26) also says that the initial and final energy levels for battery must be the same at the end of the optimization time horizon. Every battery's reactive power is also constrained by the corresponding inverter's rated capacity, modeled in eq. (27). For the safe and sustainable operation of the batteries, the energy  $B_j^t$  is constrained to be within some percentage limits of the rated battery SOC capacity, modeled using eq. (28).

#### 4.2.3 ENApp-based MPDOPF with Batteries

Assuming the presence of a feasible solution for the MPCOPF problem, the MPDOPF is formulated by decomposing the distribution system into multiple small areas. In this paper, the interaction between the two areas will follow the principle of ENApp algorithm. The ENApp algorithm leverages the radial topology of the distribution network to solve the network-level optimization problem in a distributed manner. Each area has a local controller (LC) that solves its specific local optimization problem. The local optimization

problem will be the same MPOPF as described in Section II-B but defined using only the variables and parameters specific for the corresponding area. The boundary buses between two areas are accounted as voltage sources for downstream areas and load buses for upstream areas. By knowing the upstream voltage and downstream load data, the LCs will solve their area-specific MPOPF in parallel. Once LC problem converges, the downstream and upstream LCs inform power flows and voltage data to their respective upstream and downstream areas. The LCs will again solve their local MPOPF and exchange the updated boundary variables with their neighbors. This iterative process terminates after a convergence is achieved at all boundary buses. Comprehensive details of the ENApp algorithm are available in [37]. Note that for the case of multi-period optimization with  $T$  time steps, each area exchanges a data vector containing  $2T$  boundary variables with its neighboring areas. This includes voltage and power flow data for each of the  $T$  time steps.

### 4.3 Case Study Demonstration: IEEE 123 Bus Test System

#### 4.3.1 Test System Description

The case studies are conducted on the balanced three-phase version of the IEEE 123 bus test system, which has 85 Load Nodes. Additionally, 20% (17) and 30% (26) of these load nodes also contain reactive power controllable PVs and BESS, respectively. Their ratings are as per Table 10. To demonstrate the effectiveness of the proposed algorithm, the test system is divided into four areas as shown in Fig. 4. It is assumed that a horizon-wide forecast for loads  $p_L^t$ , solar power output  $p_D^t$  and cost of substation power  $C^t$  is available to the distribution system operator. Initially, the study is carried out for 5 hours with input data shown in Fig. 5. The five-hour workflow is described below.

#### 4.3.2 Simulation Workflow

All simulations were set up in MATLAB 2023a including both the high level algorithms as well as calls to the optimization solver. MATLAB's `fmincon` function was used to parse the nonlinear nonconvex optimization problem described by eqs. (17) to (28) in tandem with the SQP optimization algorithm to solve it. From the completed simulations, the resultant optimal control variables were obtained, and were passed through an OpenDSS engine (already configured with system data and forecast values) in order to check for the ACOPF feasibility of the results. The associated code may be found in [26]. As the IEEE 123 bus system is decomposed into 4 areas, so the total number of variables exchanged at

Table 10: Parameter values

Parameter	Value
$V_{min}, V_{max}$	0.95 pu, 1.05 pu
$p_{D_{R_j}}$	$0.33p_{L_{R_j}}$
$S_{D_{R_j}}$	$1.2p_{D_{R_j}}$
$P_{B_{R_j}}$	$0.33p_{L_{R_j}}$
$S_{B_{R_j}}$	$1.2P_{B_{R_j}}$
$B_{R_j}$	$T_{fullCharge} \times P_{B_{R_j}}$
$T_{fullCharge}$	4 h
$\Delta t$	1 h
$\eta_c, \eta_d$	0.95, 0.95
$soc_{min}, soc_{max}$	0.30, 0.95
$\alpha$	0.001

each iteration for the 5-hour simulation of the MPDOPF is  $2 * 3 * 5 = 30$ .

## 4.4 Simulation Results and Performance Analysis

In the following subsections, the proposed MPDOPF algorithm is compared against the MPCOPF algorithm in terms of resultant optimal control variables, optimality gap in the objective function, and computational performance. Secondly, the resultant control variables are tested for ACOPF feasibility against OpenDSS. Section 4.4.1 describes the comparison over a 5 hour horizon with an additional focus on describing the workflow of the MPDOPF algorithm. Section 4.4.2 describes the comparison over a 10 hour horizon to test for the scalability of the MPDOPF algorithm.

### 4.4.1 5-Hour Horizon Results

Table 11 depicts a comparison between MPCOPF and MPDOPF in their problem scope, results and computational performance.

**4.4.1.1 Largest Subproblem vs. Computational Performance** This first section of the Table 11, ‘largest subproblem’ provides specifics of the ‘computational bottleneck’ encountered by either algorithm during its course. As described in Section 4.2.3, the bottleneck represents the OPF subproblem which is computationally the most intensive and thus is a

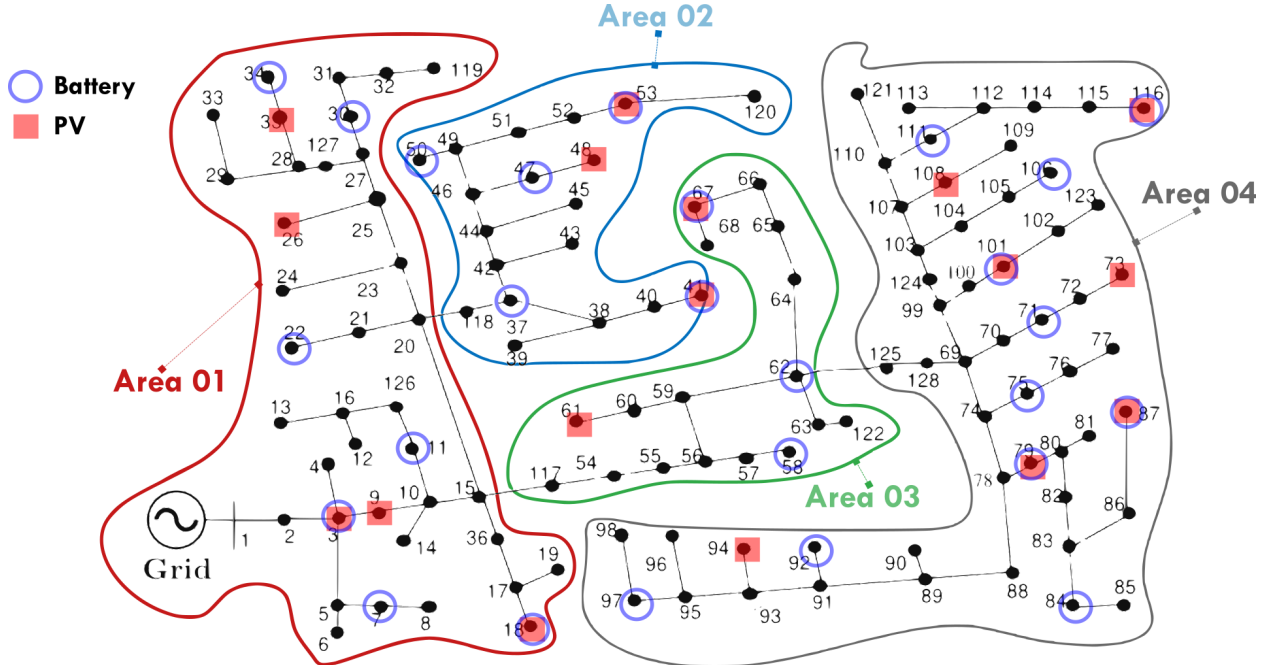


Figure 4: IEEE 123 node system divided into four areas

key indicator of the expected time the algorithm will take to complete. As can be seen in the third section ‘Computation’, there is more than a 10x speedup in computation time with MPDOPF, even though 5 such iterations were performed, totalling to 20 OPF calls over the 4 areas of the test system.

**4.4.1.2 Optimality of Objective Function and Control Variables** The second section of the Table 11 i.e. ‘Simulation results’ showcases that MPDOPF provides almost zero optimality gap (same values for Substation Power Cost, the objective function). Interestingly, there is a significant difference in the suggested optimal reactive power control values for inverters associated with DERs and batteries (results aggregated over all components over the horizon for conciseness). This highlights the fact that a nonconvex nonlinear optimization problem may not necessarily have a unique global optimal point. There is a possibility of having multiple feasible solutions with the same objective function value.

**4.4.1.3 ACOPF Feasibility Analysis** Table 12 showcases the ACOPF feasibility of the control values suggested by the MPDOPF algorithm. The first section ‘Full horizon’ describes the respective output variables for the entire horizon from MPDOPF and OpenDSS. The second section ‘Max. all-time discrepancy’ stores the highest discrepancy between key

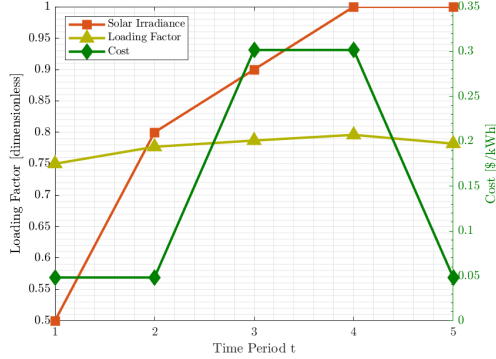


Figure 5: Forecasts for demand power, irradiance and cost of substation power over a 5 hour horizon

state/output variables for all components across any time between MPDOPF and OpenDSS. In both sections, the discrepancies are small enough to warrant the feasibility of the obtained solution.

Table 12: ACOPF feasibility analyses - 5 hour

Metric	MPDOPF	OpenDSS
Full horizon		
Substation real power (kW)	4308.14	4308.35
Line loss (kW)	76.12	76.09
Substation reactive power (kVAR)	656.24	652.49
Max. all-time discrepancy		
Voltage (pu)	0.0002	
Line loss (kW)	0.0139	
Substation power (kW)	0.3431	

To ensure that battery charging and discharging complementarity is respected without relying on integer constraints, the battery charging and discharging profiles were carefully examined. The results confirm this complementarity, as illustrated in Fig. 6 as one such example.

**4.4.1.4 Workflow Analysis** The workflow of the MPDOPF algorithm, which involves the exchange of boundary variables between parent-child area pairs, is illustrated in the convergence plots in Figs. 7 and 8. Each line graph represents a specific time period for both plots. Similarly, Fig. 9 shows the convergence of the objective function towards its optimal value over successive iterations. From these plots, we observe that although the

Table 11: Comparative analyses between MPCOPF and MPDOPF - 5 time-period horizon

Metric	MPCOPF	MPDOPF
Largest subproblem		
Decision variables	3150	1320
Linear constraints	5831	2451
Nonlinear constraints	635	265
Simulation results		
Substation power cost (\$)	576.31	576.30
Substation real power (kW)	4308.28	4308.14
Line loss (kW)	75.99	76.12
Substation reactive power (kVAR)	574.18	656.24
PV reactive power (kVAR)	116.92	160.64
Battery reactive power (kVAR)	202.73	76.01
Computation		
Number of Iterations	-	5
Total Simulation Time (s)	521.25	49.87

decision variables may initially deviate from their optimal values, they gradually approach optimality with each rolling iteration, converging after 5 macro iterations in this instance.

#### 4.4.2 10-Hour Horizon: Scalability Analysis

To demonstrate the scalability of the proposed algorithm, additional simulations were conducted over a 10-hour time horizon. Fig. 10 shows the forecasted profiles for load, solar irradiance and cost of substation power over the 10-hour horizon. The simulation results are summarized in Tables 13 and 14.

From the comparison against MPCOPF in Table 13, it can again be seen that MPDOPF is able to converge to the same optimal solution as MPCOPF. The computational speed up is even more pronounced than for the 5 time-period simulation. It was observed that the solution time for MPCOPF increased significantly with the length of the study horizon, whereas the increase in solution time for MPDOPF was comparatively smaller. This indicates that the proposed spatially distributed MPOPF framework is scalable to a certain extent.

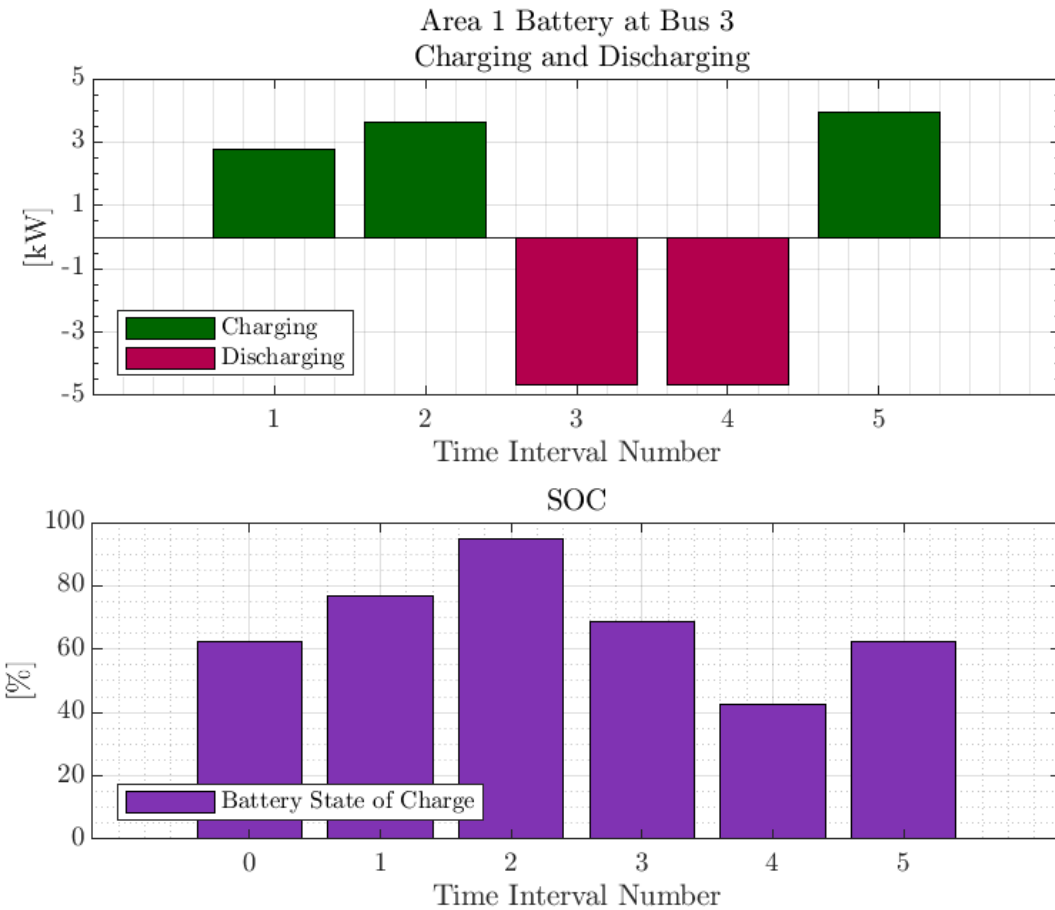


Figure 6: Charging-discharging and SOC graphs for battery at bus 3 located in Area 1 obtained by MPDOPF

Table 13: Comparison between MPCOPF and MPDOPF - 10 hour

Metric	MPCOPF	MPDOPF
Largest subproblem		
Decision variables	6300	2640
Linear constraints	11636	4891
Nonlinear constraints	1270	530
Simulation results		
Substation power cost (\$)	1197.87	1197.87
Substation real power (kW)	8544.28	8544.04
Line loss (kW)	148.67	148.94
Substation reactive power (kVAR)	1092.39	1252.03
PV reactive power (kVAR)	222.59	139.81
Battery reactive power (kVAR)	388.52	310.94
Computation	36	
Number of Iterations	-	5
Total Simulation Time (s)	4620.73	358.69

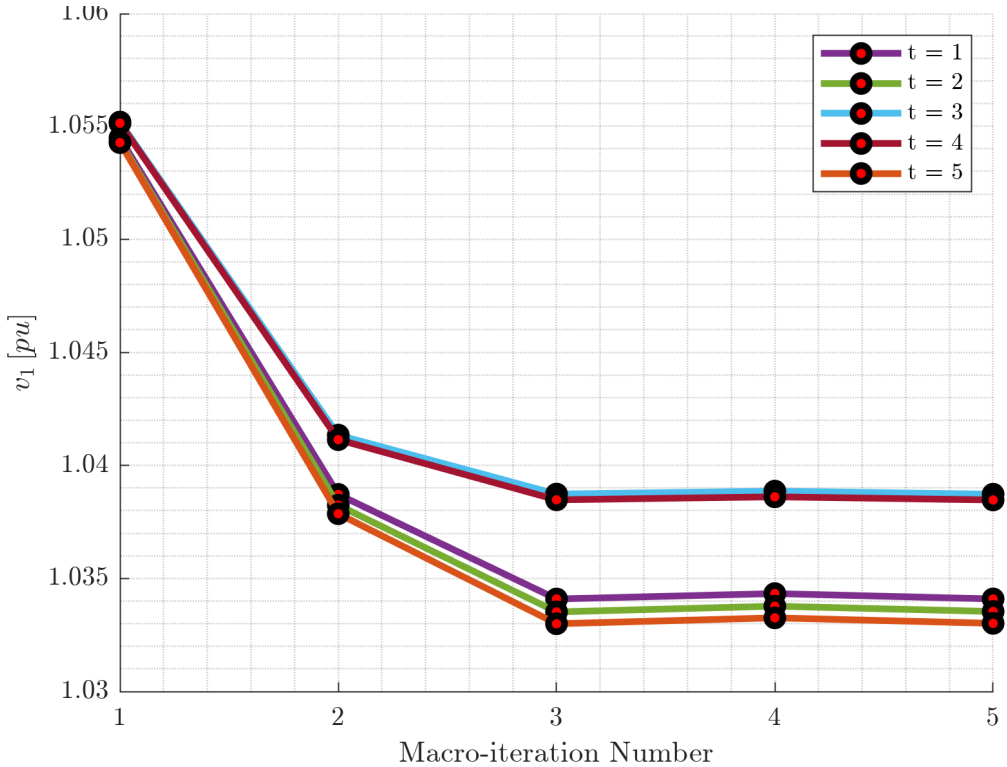


Figure 7: Shared voltage data from Area 1 to Area 2.

Again, as can be seen in Table 14 comparison against OpenDSS has yielded small discrepancies, attesting to the feasibility of the solution.

## 4.5 Summary and Discussion

The Equivalent Network Approximation (ENApp) approach provides an effective spatial decomposition framework for solving multi-period optimal power flow problems with energy storage in distribution networks. The key advantages of this approach include:

- **Computational Efficiency:** The MPDOPF algorithm achieves more than 10x speedup compared to centralized MPCOPF for medium-sized networks, with the advantage increasing for longer time horizons
- **Scalability:** The computational complexity grows more favorably with network size and time horizon length compared to centralized approaches
- **Distributed Architecture:** Each area solves its local optimization problem inde-

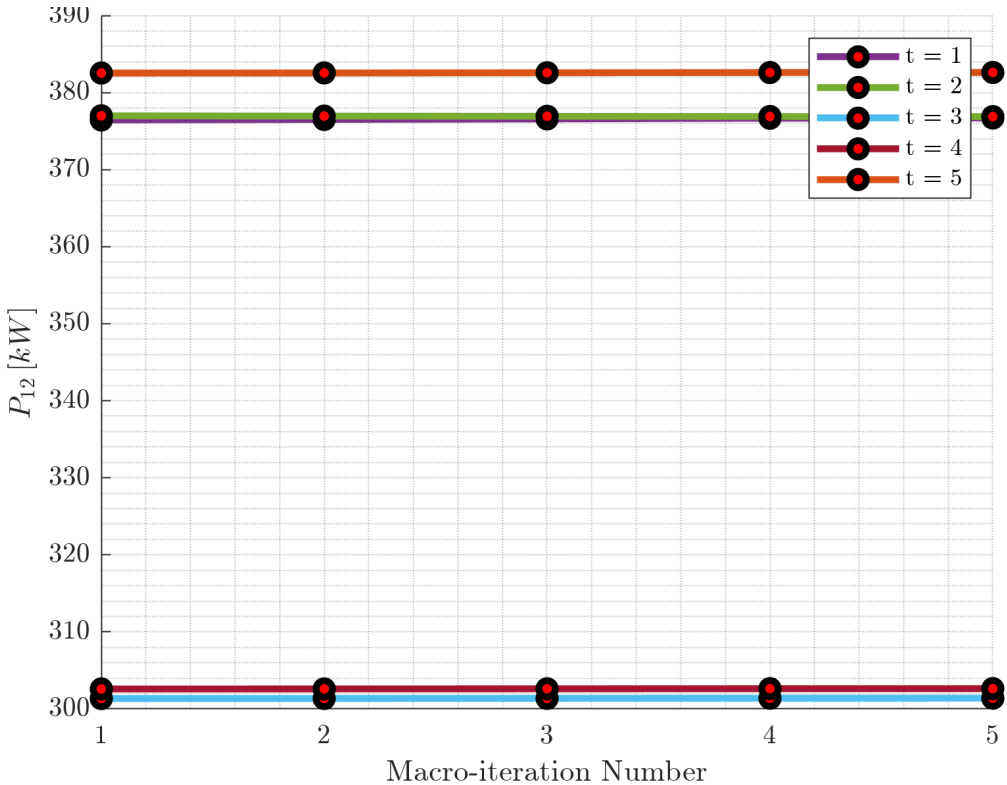


Figure 8: Shared real power data from Area 4 into Area 2.

pendently, enabling parallel computation and reducing the need for centralized data aggregation

- **Solution Quality:** The MPDOPF converges to the same optimal objective value as MPCOPF, with negligible optimality gap
- **ACOPF Feasibility:** The solutions obtained from MPDOPF are validated against OpenDSS, showing excellent agreement with acceptable discrepancies

The numerical results on the IEEE 123 bus system demonstrate that ENApp successfully decomposes the spatial network constraints while handling temporal coupling through battery SOC dynamics. The algorithm converges within a few macro iterations (typically 5), and the final solution matches the centralized optimal solution within the specified tolerances. The ACOPF feasibility analysis confirms that the obtained control variables can be implemented in practice with minimal deviation from the desired operating point.

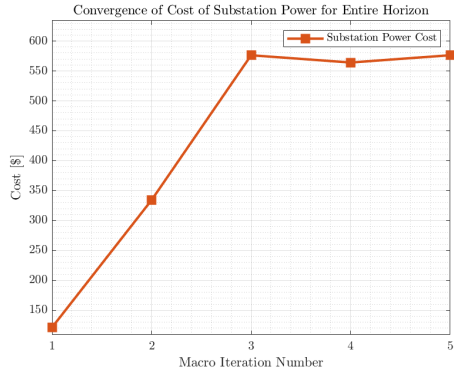


Figure 9: Convergence of objective function value with each MPDOPF iteration

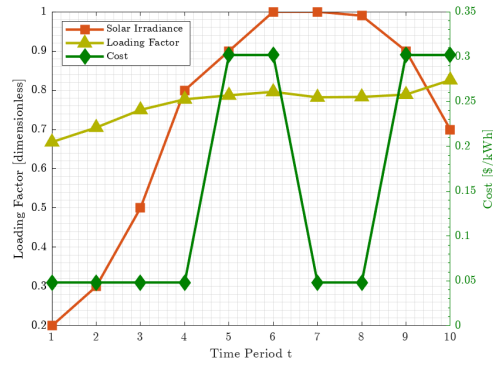


Figure 10: Forecasts for demand power, irradiance and cost of substation power over a 10 hour Horizon

#### 4.5.1 Key Observations

Several important observations emerge from the case study results:

- 1. Multiple Optimal Solutions:** The nonconvex nature of the MPOPF problem results in multiple feasible solutions with the same objective function value. This is evidenced by the different reactive power dispatch strategies between MPCOPF and MPDOPF, despite achieving the same cost.
- 2. Boundary Variable Convergence:** The convergence plots show smooth and monotonic convergence of boundary variables (voltage and power flow) across area boundaries, indicating stable numerical behavior of the ENApp algorithm.
- 3. Battery Complementarity:** The battery loss cost term successfully prevents simul-

Table 14: ACOPF feasibility analyses - 10 hour

Metric	MPDOPF	OpenDSS
Full horizon		
Substation real power (kW)	8544.04	8544.40
Line loss (kW)	148.94	148.87
Substation reactive power (kVAR)	1252.03	1243.36
Max. all-time discrepancy		
Voltage (pu)	0.0002	
Line loss (kW)	0.0132	
Substation power (kW)	0.4002	

taneous charging and discharging without requiring integer variables, simplifying the optimization problem while maintaining physical consistency.

4. **Scalability Advantage:** The computational advantage of MPDOPF becomes more pronounced as the problem size increases (from 5-hour to 10-hour horizon), demonstrating favorable scaling properties.

#### 4.5.2 Implementation Status and Future Work

The ENApp-based MPDOPF framework has been successfully implemented and validated on the IEEE 123 bus test system with realistic DER and battery penetrations. The current implementation uses the branch flow model with nonlinear constraints, solved using sequential quadratic programming (SQP) within MATLAB’s `fmincon` solver.

Future extensions of this work will focus on:

- **Larger Networks:** Applying MPDOPF to larger distribution networks (e.g., IEEE 8500 bus system) to further validate scalability
- **Higher DER Penetrations:** Testing the algorithm with increased renewable energy and battery penetrations (e.g., 50% PV, 50% BESS)
- **Uncertainty Modeling:** Incorporating stochastic or robust optimization frameworks to handle forecast uncertainties
- **Real-time Applications:** Adapting the algorithm for real-time operational decision-making with rolling horizon optimization

- **Combined Decomposition:** Integrating spatial (ENApp) and temporal (tADMM) decomposition techniques for enhanced scalability in large-scale, long-horizon problems
- **Convergence Acceleration:** Investigating adaptive parameter tuning and warm-start strategies to reduce the number of macro iterations

The successful demonstration of ENApp-based MPDOPF on realistic test cases provides a strong foundation for deploying distributed optimization algorithms in operational settings, where computational efficiency and scalability are critical requirements.

## 5 Temporal Decomposition via Temporal Alternating Direction Method of Multipliers (tADMM)

### 5.1 Introduction and Motivation

Multi-period optimal power flow (MPOPF) problems are computationally challenging due to the coupling of variables across time periods through energy storage devices, such as batteries. The temporal coupling arises from the state-of-charge (SOC) dynamics, which link the battery's energy level at each time step to its charging/discharging decisions throughout the entire planning horizon. For large-scale distribution networks with multiple time periods, solving the centralized MPOPF problem becomes intractable.

The Alternating Direction Method of Multipliers (ADMM) is a powerful decomposition technique for solving large-scale convex optimization problems [42, 43]. ADMM is particularly effective for problems that can be decomposed into smaller, more manageable subproblems. The temporal ADMM (tADMM) approach adapts the classical ADMM framework to decompose the MPOPF problem across the temporal dimension, enabling parallel computation of individual time-step subproblems while maintaining consensus on the battery SOC trajectories.

The key insight of tADMM is that while spatial network constraints (power flow equations, voltage limits) are local to each time step, the temporal coupling through battery SOC can be handled through consensus variables. Each time-step subproblem maintains its own local copy of the battery SOC trajectory, and these local copies are coordinated through a global consensus variable that is updated iteratively. This decomposition structure allows for:

- **Parallel computation:** Each time-step subproblem can be solved independently and in parallel
- **Scalability:** Computational complexity grows more favorably with the number of time periods compared to centralized approaches
- **Modularity:** The framework can accommodate different network models (LinDist-Flow, copper plate) without changing the decomposition structure

## 5.2 LinDistFlow MPOPF with tADMM

### 5.2.1 Problem Overview

The Temporal ADMM (tADMM) algorithm decomposes the multi-period optimal power flow problem for distribution networks into  $T$  subproblems, each corresponding to one time period. This formulation uses the linearized DistFlow model to capture network physics including voltage drops and reactive power flows. The algorithm maintains consensus on battery state-of-charge (SOC) trajectories across all subproblems through an iterative update procedure.

### 5.2.2 Variable Color Coding

To clearly distinguish the different types of variables in the tADMM formulation, we use the following color-coding scheme:

- $\mathbf{B}_j^{t_0}[t]$  (Blue): Local SOC variables for battery  $j$  in subproblem  $t_0$ , evaluated at time  $t$ . These are the primal variables optimized in each subproblem.
- $\hat{\mathbf{B}}_j[t]$  (Red): Global consensus SOC for battery  $j$  at time  $t$ . This represents the agreed-upon SOC trajectory that all subproblems aim to converge to.
- $\mathbf{u}_j^{t_0}[t]$  (Green): Local scaled dual variables for battery  $j$  in subproblem  $t_0$ , for time  $t$ . These accumulate the consensus violation and guide convergence.

### 5.2.3 Sets and Indices

- $\mathcal{N}$ : Set of all nodes (buses)
- $\mathcal{L}$ : Set of all branches (lines)
- $\mathcal{L}_1$ : Set of branches connected to substation (node 1)
- $\mathcal{B}$ : Set of nodes with batteries
- $\mathcal{D}$ : Set of nodes with PV (DER)
- $\mathcal{T} = \{1, 2, \dots, T\}$ : Set of time periods
- $t_0 \in \mathcal{T}$ : Index for a specific time period in tADMM decomposition

- $j \in \mathcal{N}$ : Node index
- $(i, j) \in \mathcal{L}$ : Branch from node  $i$  to node  $j$

#### 5.2.4 tADMM Algorithm Structure

The tADMM algorithm follows the consensus-based ADMM framework [42, 43], where the true global problem involves a single consensus variable that is used (partially or fully) by all individual subproblems. In the context of MPOPF, the consensus variable is the battery SOC trajectory, and each time-step subproblem maintains its own local copy of this trajectory.

The algorithm alternates between three update steps at each iteration  $k$ :

**5.2.4.1 Step 1: Subproblem Update (Blue Variables)** In the first update step, we solve each subproblem  $t_0 \in \{1, 2, \dots, T\}$  independently and in parallel. Each subproblem optimizes its local copy of the battery SOC trajectory  $\mathbf{B}_j^{\text{to}}[\mathbf{t}]$  along with the network variables for its specific time step. The latest values of the global consensus variable  $\hat{\mathbf{B}}_j[\mathbf{t}]$  and dual variables  $\mathbf{u}_j^{\text{to}}[\mathbf{t}]$  from the previous iteration are used to guide the optimization toward consensus.

For each subproblem  $t_0 \in \{1, 2, \dots, T\}$ :

$$\begin{aligned} & \min_{\substack{P_{\text{Subs}}^{t_0}, Q_{\text{Subs}}^{t_0}, \\ P_{ij}^{t_0}, Q_{ij}^{t_0}, v_j^{t_0}, q_{D,j}^{t_0, \\ P_{B,j}^t, \mathbf{B}_j^{\text{to}}[\mathbf{t}], \\ \forall j \in \mathcal{B}, t \in \mathcal{T}}} c^{t_0} \cdot P_{\text{Subs}}^{t_0} \cdot P_{\text{BASE}} \cdot \Delta t + C_B \sum_{j \in \mathcal{B}} (P_{B,j}^{t_0})^2 \cdot P_{\text{BASE}}^2 \cdot \Delta t \\ & + \frac{\rho}{2} \sum_{j \in \mathcal{B}} \sum_{t=1}^T \left( \mathbf{B}_j^{\text{to}}[\mathbf{t}] - \hat{\mathbf{B}}_j[\mathbf{t}] + \mathbf{u}_j^{\text{to}}[\mathbf{t}] \right)^2 \end{aligned} \quad (29)$$

**Subject to:**

**Spatial Network Constraints (only for time  $t_0$ ):**

$$\text{Real power balance (substation): } P_{\text{Subs}}^{t_0} - \sum_{(1,j) \in \mathcal{L}_1} P_{1j}^{t_0} = 0 \quad (30)$$

$$\begin{aligned} \text{Real power balance (nodes): } P_{ij}^{t_0} - \sum_{(j,k) \in \mathcal{L}} P_{jk}^{t_0} &= P_{B,j}^{t_0} + p_{D,j}^{t_0} - p_{L,j}^{t_0}, \\ &\forall (i, j) \in \mathcal{L}, \end{aligned} \quad (31)$$

$$\text{Reactive power balance (substation): } Q_{\text{Subs}}^{t_0} - \sum_{(1,j) \in \mathcal{L}_1} Q_{1j}^{t_0} = 0 \quad (32)$$

$$\begin{aligned} \text{Reactive power balance (nodes): } Q_{ij}^{t_0} - \sum_{(j,k) \in \mathcal{L}} Q_{jk}^{t_0} &= q_{D,j}^{t_0} - q_{L,j}^{t_0}, \\ &\forall (i, j) \in \mathcal{L}, \end{aligned} \quad (33)$$

$$\text{KVL constraints: } v_i^{t_0} - v_j^{t_0} = 2(r_{ij}P_{ij}^{t_0} + x_{ij}Q_{ij}^{t_0}), \quad \forall (i, j) \in \mathcal{L} \quad (34)$$

$$\text{Voltage limits: } (V_{\min,j})^2 \leq v_j^{t_0} \leq (V_{\max,j})^2, \quad \forall j \in \mathcal{N} \quad (35)$$

$$\begin{aligned} \text{PV reactive limits: } -\sqrt{(S_{D,j})^2 - (p_{D,j}^{t_0})^2} &\leq q_{D,j}^{t_0} \leq \sqrt{(S_{D,j})^2 - (p_{D,j}^{t_0})^2}, \\ &\forall j \in \mathcal{D} \end{aligned} \quad (36)$$

**Temporal Battery Constraints (entire horizon  $t \in \{1, \dots, T\}$ ):**

$$\text{Initial SOC: } \mathbf{B}_j^{\text{to}}[\mathbf{1}] = B_{0,j} - P_{B,j}^1 \cdot \Delta t, \quad \forall j \in \mathcal{B} \quad (37)$$

$$\text{SOC trajectory: } \mathbf{B}_j^{\text{to}}[\mathbf{t}] = \mathbf{B}_j^{\text{to}}[\mathbf{t-1}] - P_{B,j}^t \cdot \Delta t, \quad \forall t \in \{2, \dots, T\}, j \in \mathcal{B} \quad (38)$$

$$\begin{aligned} \text{SOC limits: } \text{SOC}_{\min,j} \cdot B_{\text{rated},j} &\leq \mathbf{B}_j^{\text{to}}[\mathbf{t}] \leq \text{SOC}_{\max,j} \cdot B_{\text{rated},j}, \\ &\forall t \in \mathcal{T}, j \in \mathcal{B} \end{aligned} \quad (39)$$

$$\text{Power limits: } -P_{B,\text{rated},j} \leq P_{B,j}^t \leq P_{B,\text{rated},j}, \quad \forall t \in \mathcal{T}, j \in \mathcal{B} \quad (40)$$

**Key Formulation Notes:**

- **Network variables** ( $P_{\text{Subs}}^{t_0}, Q_{\text{Subs}}^{t_0}, P_{ij}^{t_0}, Q_{ij}^{t_0}, v_j^{t_0}, q_{D,j}^{t_0}$ ) are optimized *only* for time step  $t_0$ , representing the spatial network state at that particular time
- **Battery power**  $P_{B,j}^t$  is optimized for the *entire* horizon  $t \in \{1, \dots, T\}$  to allow proper accounting of temporal coupling
- **Local SOC trajectory**  $\mathbf{B}_j^{\text{to}}[\mathbf{t}]$  is computed for *all* time steps  $t \in \{1, \dots, T\}$  based on the battery power decisions

- The ADMM consensus penalty compares the full local trajectory  $\mathbf{B}_j^{\text{to}}[\mathbf{t}]$  with the global master copy  $\hat{\mathbf{B}}_j[\mathbf{t}]$ , penalized by the dual variables  $\mathbf{u}_j^{\text{to}}[\mathbf{t}]$
- Each battery  $j \in \mathcal{B}$  has its own set of local/global SOC variables and dual variables

**5.2.4.2 Step 2: Consensus Update (Red Variables)** After all subproblems have been solved in parallel to obtain the latest values of  $\mathbf{B}_j^{\text{to}}[\mathbf{t}]$ , the global consensus variable  $\hat{\mathbf{B}}_j[\mathbf{t}]$  is updated by averaging the local SOC trajectories across all subproblems, adjusted by the dual variables. This update brings the consensus closer to the average of what each subproblem believes the SOC should be.

For each battery  $j \in \mathcal{B}$  and each time period  $t \in \mathcal{T}$ :

$$\hat{\mathbf{B}}_j[\mathbf{t}] = \text{clamp} \left( \frac{1}{T} \sum_{t_0=1}^T (\mathbf{B}_j^{\text{to}}[\mathbf{t}] + \mathbf{u}_j^{\text{to}}[\mathbf{t}]), \underline{B}_j, \bar{B}_j \right) \quad (41)$$

where  $\underline{B}_j = \text{SOC}_{\min,j} \cdot B_{\text{rated},j}$  and  $\bar{B}_j = \text{SOC}_{\max,j} \cdot B_{\text{rated},j}$ . The clamping operation ensures that the consensus variable respects the physical SOC bounds.

**5.2.4.3 Step 3: Dual Update (Green Variables)** Finally, the dual variables  $\mathbf{u}_j^{\text{to}}[\mathbf{t}]$  are updated to accumulate the consensus violation (the difference between local and global SOC). These dual variables act as Lagrange multipliers that enforce consensus in the limit as the algorithm converges.

For each battery  $j \in \mathcal{B}$ , each subproblem  $t_0 \in \mathcal{T}$ , and each time period  $t \in \mathcal{T}$ :

$$\mathbf{u}_j^{\text{to}}[\mathbf{t}] := \mathbf{u}_j^{\text{to}}[\mathbf{t}] + (\mathbf{B}_j^{\text{to}}[\mathbf{t}] - \hat{\mathbf{B}}_j[\mathbf{t}]) \quad (42)$$

These three steps are repeated iteratively: solve subproblems for **blue variables**, update consensus **red variables**, and update dual **green variables**, until convergence is achieved.

## 5.2.5 Convergence Criteria

### Primal Residual (Consensus Violation):

The primal residual measures how well the local SOC trajectories  $\mathbf{B}_j^{\text{to}}[\mathbf{t}]$  agree with the global consensus  $\hat{\mathbf{B}}_j[\mathbf{t}]$  across all batteries and time steps.

$$\|r^k\|_2 = \frac{1}{|\mathcal{B}|} \sqrt{\sum_{j \in \mathcal{B}} \sum_{t=1}^T \left( \frac{1}{T} \sum_{t_0=1}^T \mathbf{B}_j^{t_0}[\mathbf{t}] - \hat{\mathbf{B}}_j[\mathbf{t}] \right)^2} \leq \epsilon_{\text{pri}} \quad (43)$$

#### Dual Residual (Consensus Change):

The dual residual measures the change in the consensus variable between iterations, indicating convergence stability.

$$\|s^k\|_2 = \frac{\rho}{|\mathcal{B}|} \sqrt{\sum_{j \in \mathcal{B}} \sum_{t=1}^T \left( \hat{\mathbf{B}}_j^k[\mathbf{t}] - \hat{\mathbf{B}}_j^{k-1}[\mathbf{t}] \right)^2} \leq \epsilon_{\text{dual}} \quad (44)$$

### 5.3 Copper Plate MPOPF with tADMM (Simplified Case)

#### 5.3.1 Problem Overview

To illustrate the tADMM framework more clearly, we first present a simplified copper plate model where network constraints are neglected, and only a single aggregate power balance is enforced at each time step. The Temporal ADMM (tADMM) algorithm decomposes the multi-period optimal power flow problem into  $T$  single-step subproblems, each corresponding to one time period. The hope is to enable parallel computation and improved scalability while still retaining solution optimality. Fig. 11 shows the input data for a 24-hour horizon, including the time-varying electricity cost and load demand profiles used in the copper plate MPOPF formulation.

#### 5.3.2 Variable Color Coding

- $\mathbf{B}^{t_0}$  (Blue): Local SOC variables for subproblem  $t_0$
- $\hat{\mathbf{B}}$  (Red): Global consensus SOC trajectory
- $\mathbf{u}^{t_0}$  (Green): Local scaled dual variables for subproblem  $t_0$

#### 5.3.3 tADMM Algorithm Structure

The algorithm alternates between three update steps following the consensus ADMM framework [42, 43]:

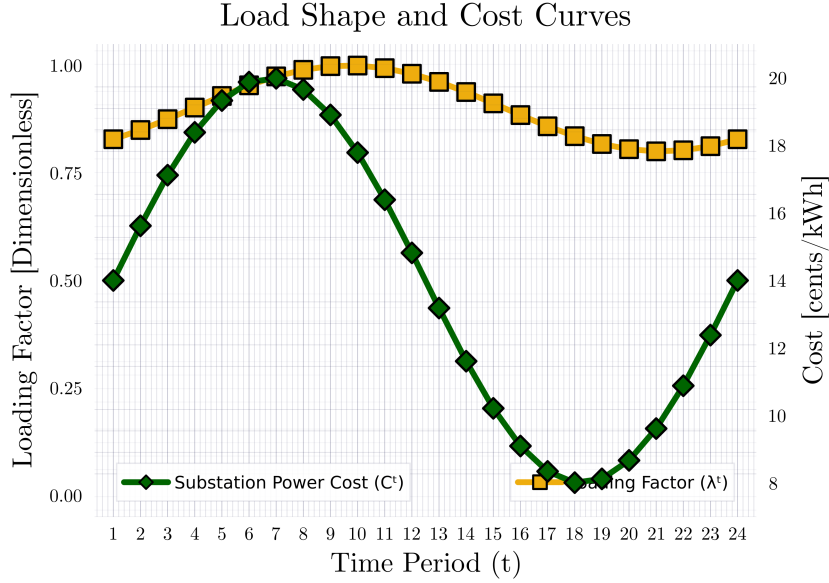


Figure 11: Input curves showing electricity cost and load demand over a 24-hour period.

### 5.3.3.1 Step 1: Primal Update (Blue Variables) - tADMM Optimization Model

In Update 1 (at iteration  $k$ ), the latest values of subproblem copies are solved for in parallel using the last known copies of the consensus variable and dual variables – namely  $\hat{\mathbf{B}}^{k-1}$  and  $\mathbf{u}^{t_0, k-1}$ , respectively.

For each subproblem  $t_0 \in \{1, 2, \dots, T\}$ :

$$\min_{P_{\text{subs}}^{t_0}, P_B^{t_0}, \mathbf{B}^{t_0}} C^{t_0} \cdot P_{\text{subs}}^{t_0} + C_B \cdot (P_B^{t_0})^2 + \frac{\rho}{2} \left\| \mathbf{B}^{t_0} - \hat{\mathbf{B}} + \mathbf{u}^{t_0} \right\|_2^2 \quad (45)$$

**Subject to SOC Dynamics for Entire Trajectory:**

$$\mathbf{B}^{t_0}[1] = B_0 - P_B^{t_0} \cdot \Delta t \quad (46)$$

$$\mathbf{B}^{t_0}[t] = \mathbf{B}^{t_0}[t-1] - P_B^{t_0} \cdot \Delta t, \quad \forall t \in \{2, \dots, T\} \quad (47)$$

$$P_{\text{subs}}^{t_0} + P_B^{t_0} = P_L[t_0] \quad (48)$$

$$-P_{B,R} \leq P_B^{t_0} \leq P_{B,R} \quad (49)$$

$$\underline{B} \leq \mathbf{B}^{t_0}[t] \leq \bar{B}, \quad \forall t \in \{1, \dots, T\} \quad (50)$$

**Key Formulation Notes:**

- Each subproblem  $t_0$  optimizes the battery power  $P_B^{t_0}$  for *only* time step  $t_0$
- However, the SOC trajectory  $\mathbf{B}^{\text{to}}[\mathbf{t}]$  is computed for *all* time steps  $t \in \{1, \dots, T\}$
- This ensures that the ADMM penalty term can compare the full trajectory  $\mathbf{B}^{\text{to}}$  with the consensus  $\hat{\mathbf{B}}$
- The power balance constraint is enforced only for the specific time  $t_0$

**5.3.3.2 Step 2: Consensus Update (Red Variables)** In Update 2 (at iteration  $k$ ), the latest value of the global consensus variable is computed using the last known copies of the local subproblem SOC trajectories and dual variables – namely  $\mathbf{B}_i^{\text{to},k}$  and  $\mathbf{u}_i^{\text{to},k-1}$ , respectively.

$$\hat{\mathbf{B}}[\mathbf{t}] = \text{clamp} \left( \frac{1}{T} \sum_{t_0=1}^T (\mathbf{B}^{\text{to}}[\mathbf{t}] + \mathbf{u}^{\text{to}}[\mathbf{t}]), \underline{B}, \bar{B} \right) \quad (51)$$

$$\forall t \in \{1, 2, \dots, T-1\} \quad (52)$$

$$\hat{\mathbf{B}}[\mathbf{T}] = B_{T,\text{target}} \quad (\text{if terminal constraint exists}) \quad (53)$$

**5.3.3.3 Step 3: Dual Update (Green Variables)** In Update 3 (at iteration  $k$ ), the latest values of local dual variables are computed using the last known copies of the local SOC, global consensus, and previous dual variables – namely  $\mathbf{B}_i^{\text{to},k}$ ,  $\hat{\mathbf{B}}^k$ , and  $\mathbf{u}_i^{\text{to},k-1}$ , respectively.

$$\mathbf{u}^{\text{to}}[\mathbf{t}] := \mathbf{u}^{\text{to}}[\mathbf{t}] + (\mathbf{B}^{\text{to}}[\mathbf{t}] - \hat{\mathbf{B}}[\mathbf{t}]) \quad (54)$$

$$\forall t_0 \in \{1, \dots, T\}, \forall t \in \{1, \dots, T\} \quad (55)$$

After every subproblem is solved once to get the latest values of  $\mathbf{B}_1, \mathbf{B}_2, \dots, \mathbf{B}_B$ , the value of the consensus variable  $\hat{\mathbf{B}}$  is updated. Next, the dual variables  $\mathbf{u}_1, \mathbf{u}_2, \dots, \mathbf{u}_B$  are updated. This process repeats until convergence.

## 5.4 Numerical Results

### 5.4.1 Battery Actions and Convergence Analysis

To validate the tADMM approach, we present numerical results for the copper plate MPOPF problem with a 24-hour planning horizon. The test case includes a single battery energy storage system with time-varying electricity prices and load demands as shown in Fig. 11.

Fig. 12 shows the optimal battery charging and discharging actions obtained from solving the centralized (brute force) MPOPF problem. The battery strategically charges during low-cost periods (typically during nighttime and early morning hours) and discharges during high-cost periods (peak demand hours in the afternoon and evening) to minimize the overall energy cost over the 24-hour horizon. This behavior demonstrates the value of energy arbitrage enabled by battery storage.

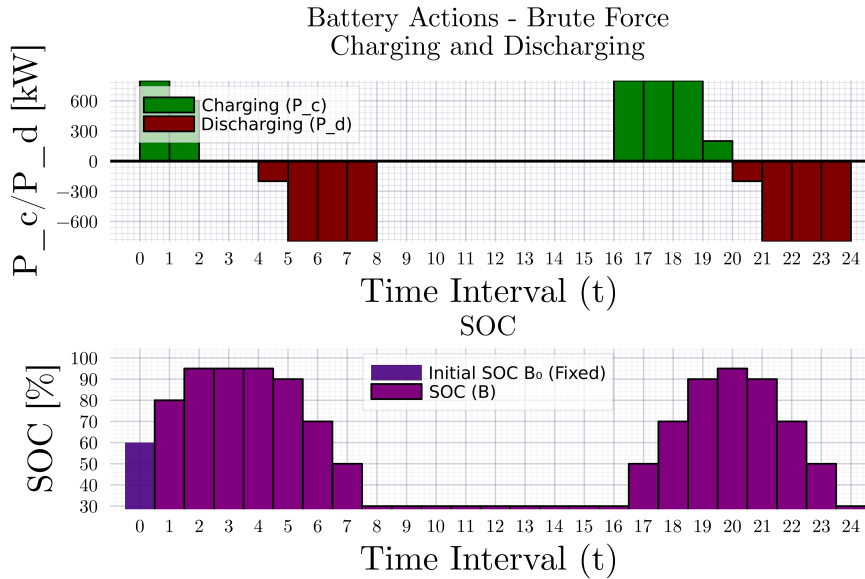


Figure 12: Optimal battery power actions (brute force centralized solution) for copper plate MPOPF over 24-hour horizon. Positive values indicate discharging (supplying power), while negative values indicate charging (consuming power).

Fig. 13 presents the battery actions obtained using the tADMM algorithm, demonstrating that the decomposition approach converges to a solution that closely matches the centralized optimal solution. The close agreement between the two solutions validates the effectiveness of the tADMM decomposition for this problem class. Minor differences, if any, are within the specified convergence tolerances.

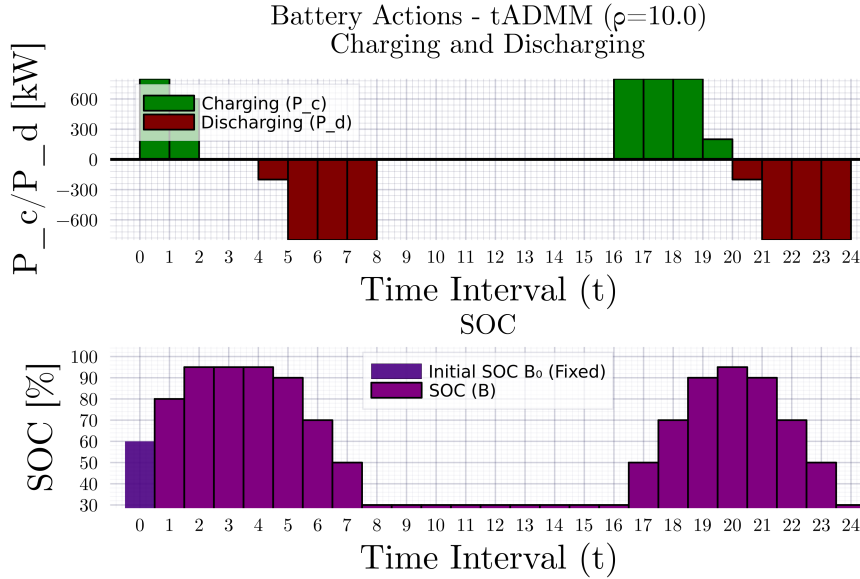


Figure 13: Battery power actions obtained using tADMM for copper plate MPOPF over 24-hour horizon. The solution converges to match the centralized optimal solution.

Fig. 14 illustrates the convergence behavior of the tADMM algorithm, showing how the primal and dual residuals decrease over iterations until they satisfy the specified convergence tolerances ( $\epsilon_{\text{pri}} = 10^{-3}$  and  $\epsilon_{\text{dual}} = 10^{-3}$ ). The algorithm typically converges within a few dozen iterations, demonstrating good computational efficiency. The primal residual (consensus violation) decreases as the local SOC trajectories  $\mathbf{B}^{t_0}$  converge to the global consensus  $\hat{\mathbf{B}}$ , while the dual residual tracks the stability of the consensus variable across iterations.

## 5.5 Convergence Criteria

The algorithm terminates when both residuals fall below specified thresholds:

### 5.5.1 Convergence Criteria

The algorithm terminates when both residuals fall below specified thresholds:

#### Primal Residual (Consensus Violation):

The primal residual measures how well the local SOC trajectories  $\mathbf{B}^{t_0}$  agree with the global consensus  $\hat{\mathbf{B}}$ . A small primal residual indicates that all subproblems have converged to a consistent SOC trajectory.

$$\|r^k\|_2 = \left\| \text{vec} \left( \left\{ \mathbf{B}^{t_0} - \hat{\mathbf{B}} \right\}_{t_0=1}^T \right) \right\|_2 \leq \epsilon_{\text{pri}} \quad (56)$$

### Dual Residual (Consensus Change):

The dual residual measures how much the consensus variable  $\hat{\mathbf{B}}$  is changing between iterations. A small dual residual indicates that the consensus has stabilized.

$$\|s^k\|_2 = \rho \left\| \hat{\mathbf{B}}^k - \hat{\mathbf{B}}^{k-1} \right\|_2 \leq \epsilon_{\text{dual}} \quad (57)$$

## 5.6 Algorithm Parameters

### 5.6.1 Objective Function Components

The tADMM objective function for each subproblem  $t_0$  consists of three terms:

$$\text{Energy Cost: } C^{t_0} \cdot P_{\text{subs}}^{t_0} \cdot \Delta t \quad (58)$$

$$\text{Battery Quadratic Cost: } C_B \cdot (P_B^{t_0})^2 \cdot \Delta t \quad (59)$$

$$\text{ADMM Penalty: } \frac{\rho}{2} \left\| B^{t_0} - \hat{B} + u^{t_0} \right\|_2^2 \quad (60)$$

Where:

- $C^{t_0}$ : Energy price at time  $t_0$  [\$/kWh]
- $C_B$ : Battery quadratic cost coefficient [\$/kW<sup>2</sup>/h] (typically  $10^{-6} \times \min(C^t)$ )
- $\rho$ : ADMM penalty parameter

The battery quadratic cost term  $C_B \cdot (P_B^{t_0})^2$  serves as a regularization to:

1. Prevent excessive battery cycling
2. Encourage smoother power trajectories
3. Improve numerical conditioning of the optimization problem

### 5.6.2 Algorithmic Parameters

- **Penalty Parameter:**  $\rho$  (typically 0.1 to 10.0)
- **Primal Tolerance:**  $\epsilon_{\text{pri}} = 10^{-3}$
- **Dual Tolerance:**  $\epsilon_{\text{dual}} = 10^{-3}$
- **Maximum Iterations:** 1000

## 5.7 Appendix: Full Variable and Parameter Definitions

### 5.7.1 System Bases

$$\text{kV}_B = \frac{4.16}{\sqrt{3}} \text{ kV} \text{ (phase-to-neutral)} \quad (61)$$

$$\text{kVA}_B = 1000 \text{ kVA} \quad (62)$$

$$P_{\text{BASE}} = 1000 \text{ kW} \quad (63)$$

$$E_{\text{BASE}} = 1000 \text{ kWh per hour} \quad (64)$$

### 5.7.2 SOC Bound Definitions

$$\underline{B} = \text{SOC}_{\min} \cdot E_{\text{Rated}} \quad (65)$$

$$\overline{B} = \text{SOC}_{\max} \cdot E_{\text{Rated}} \quad (66)$$

### 5.7.3 Physical Interpretation

- $P_B[t] > 0$ : Battery discharging (providing power to the system)
- $P_B[t] < 0$ : Battery charging (consuming power from the system)
- $B[t]$ : Battery state of charge at the end of period  $t$
- $\underline{B} = \text{SOC}_{\min} \cdot E_{\text{Rated}}$ : Lower SOC bound
- $\overline{B} = \text{SOC}_{\max} \cdot E_{\text{Rated}}$ : Upper SOC bound

## 5.8 Summary and Discussion

The temporal ADMM (tADMM) approach provides an effective decomposition framework for solving multi-period optimal power flow problems with energy storage. The key advantages of this approach include:

- **Parallelization:** Each time-step subproblem can be solved independently and in parallel, enabling computational speedup on multi-core processors or distributed computing platforms
- **Modularity:** The decomposition structure is flexible and can accommodate different network models (LinDistFlow, AC power flow, copper plate) without changing the temporal decomposition framework
- **Scalability:** The computational complexity scales more favorably with the number of time periods compared to solving the full centralized problem
- **Convergence guarantees:** For convex formulations, ADMM provides theoretical convergence guarantees to the global optimum [42, 43]

The numerical results demonstrate that tADMM successfully decomposes the temporal coupling through battery SOC while maintaining solution optimality. The algorithm converges within a reasonable number of iterations, and the final solution matches the centralized optimal solution within the specified tolerances. This validates the effectiveness of the consensus-based decomposition for handling temporal coupling in MPOPF problems.

### 5.8.1 Implementation Status

The tADMM framework has been developed and tested with varying levels of network model complexity:

- **Copper Plate Model (Completed):** The tADMM algorithm has been successfully implemented and tested for the simplified copper plate MPOPF problem. The numerical results presented in Figs. 12, 13, and 14 demonstrate successful convergence to the optimal solution, validating the temporal decomposition approach.
- **LinDistFlow Model (In Progress):** The tADMM formulation with the linearized DistFlow model [44] is currently being implemented. This will incorporate spatial

network constraints including voltage limits, line flow limits, and reactive power constraints while maintaining the temporal decomposition structure.

- **Nonlinear Branch Flow Model (Planned):** Future work will extend the tADMM framework to the SOCP-relaxed nonlinear branch flow model (BFM) [4]. This represents the true nonlinear MPOPF problem with exact AC power flow physics. The BFM formulation will provide a more accurate representation of distribution network behavior while benefiting from the computational advantages of temporal decomposition. This will showcase the full potential of tADMM for solving realistic large-scale MPOPF problems with complex network constraints.

Future extensions of this work will focus on:

- Completing the LinDistFlow implementation and validating performance on realistic distribution networks
- Implementing the SOCP-relaxed BFM formulation with tADMM decomposition
- Applying tADMM to larger distribution networks with multiple batteries and renewable energy sources
- Investigating adaptive penalty parameter selection strategies to improve convergence speed
- Integrating spatial decomposition techniques with temporal decomposition for enhanced scalability

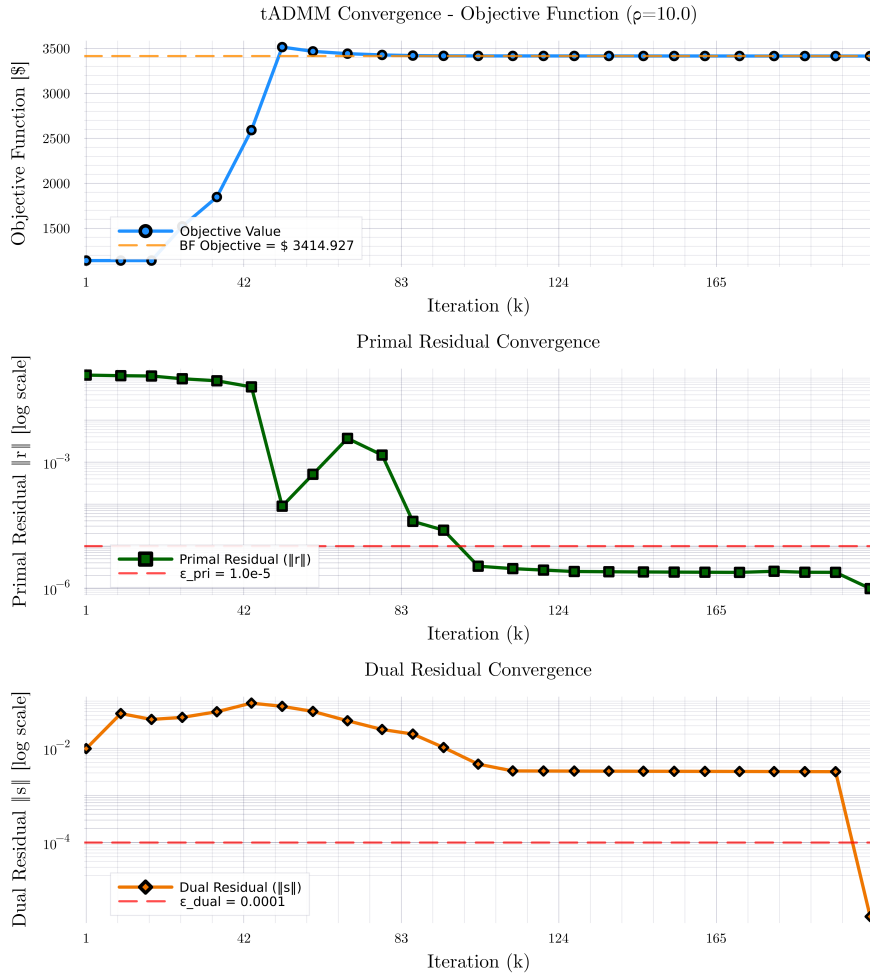


Figure 14: Convergence curves showing primal and dual residuals for tADMM algorithm.

## 6 Future Works

The proposed future work aims to extend the temporal decomposition framework developed in this research to larger and more complex power distribution systems. The timeline for completion spans three semesters from Fall 2025 through Summer 2026, culminating in dissertation preparation and defense. The work is organized into three main tasks that progressively scale the methodology and conclude the doctoral research.

### 6.1 Task 1: Temporal Decomposition for Medium Sized Balanced Three-Phase Systems

The first task focuses on developing and validating the temporal decomposition approach for medium-scale distribution systems assuming balanced three-phase conditions. So far the mathematical framework for temporal decomposition using tADMM has been established, extending the concepts developed in earlier work to handle time-coupled constraints and multi-period optimization problems. The formulation phase will establish the theoretical foundations and decomposition strategy.

Following the formulation, implementation and testing will be conducted on the IEEE 123-bus single-phase test system. This medium-scale system provides sufficient complexity to validate the decomposition approach while remaining computationally tractable for initial testing. The implementation will focus on developing efficient algorithms and testing convergence properties. This task is scheduled for completion during Fall 2025.

### 6.2 Task 2: Temporal Decomposition for Large Sized Unbalanced Three-Phase Systems

The second task scales the temporal decomposition methodology to large-scale three-phase distribution systems. Building on the insights from Task 1, this phase will formulate the decomposition approach specifically for three-phase unbalanced systems, accounting for the additional complexity of phase coupling and imbalance.

The implementation and testing will be performed on the IEEE 9500-bus three-phase test system, which represents a realistic large-scale distribution network. This task will demonstrate the scalability of the temporal decomposition approach and validate its effectiveness on industry-relevant system sizes. The work is planned for completion during Spring 2026.

### **6.3 Task 3: Concluding Research and Dissertation**

The final task encompasses completion of remaining research activities and dissertation preparation. This includes finishing the investigation of differential dynamic programming (DDP) methods, conducting a comprehensive literature review on novel temporal decomposition methods in power systems, and completing any remaining implementations or case studies.

The dissertation preparation and defense phase will synthesize all research contributions, document the methodologies and results, and prepare for the final defense. This task spans from late Spring 2026 through Summer 2026, concluding the doctoral research program.

## 6.4 Timeline

The timeline for the research efforts as detailed in Section 6 is shown in Fig. 15.

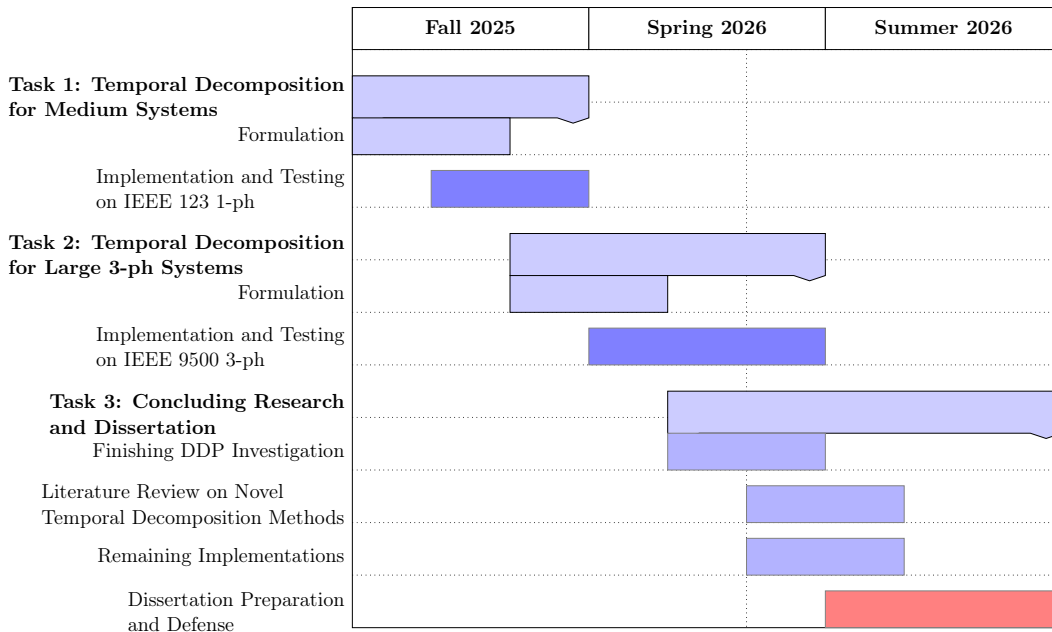


Figure 15: Gantt chart showing execution plan for future works.

## 7 Biography

Aryan Ritwajeet Jha received the B.E. degree in Electrical and Electronics Engineering from the Birla Institute of Technology and Science (BITS) Pilani, India, in 2020. He is currently pursuing his Ph.D. in Electrical Engineering at Washington State University, Pullman, WA, USA. His research interests include power distribution system optimization, scalable decomposition algorithms for large-scale non-linear optimization and optimization solvers.

### 7.1 Publications

1. **Jha, A. R.**, Paul, S., & Dubey, A. . Spatially Distributed Multi-Period Optimal Power Flow with Battery Energy Storage Systems. 2024 56th North American Power Symposium (NAPS). IEEE. doi: 10.1109/NAPS61145.2024.10741846 [1]
2. **Jha, A. R.**, Paul, S., & Dubey, A. . Analyzing the Performance of Linear and Nonlinear Multi -Period Optimal Power Flow Models for Active Distribution Networks. 2025 IEEE North-East India International Energy Conversion Conference and Exhibition (NE-IECCE). IEEE. doi: 10.1109/NE-IECCE64154.2025.11183479 [8]

## 7.2 Program of Study Course Work

Course Number and Name	Semester	Instructor	Grade
E_E 507 Random Processes in Engineering	Fall 2022	Prof. Sandip Roy	A
E_E 521 Analysis of Power Systems	Fall 2022	Prof. Noel Schulz	A
E_E 523 Power Systems Stability	Spring 2023	Prof. Mani V. Venkatasubramanian	A
MATH 564 Convex and Nonlinear Optimization	Fall 2023	Prof. Tom Asaki	A
MATH 565 Nonsmooth Analysis and Optimization	Spring 2024	Prof. Tom Asaki	A-
CPT_S 530 Numerical Analysis <sup>1</sup>	Fall 2025	Prof. Alexander Panchenko	
E_E 582 Electrical Systems Modelling and Simulation <sup>1</sup>	Fall 2025	Prof. Seyedmilad Ebrahimi	
E_E 595 Directed Studies in Electrical Engineering <sup>1</sup>	Fall 2025	Prof. Rahul K. Gupta	

<sup>1</sup>

---

<sup>1</sup>currently taking this semester

# Appendix

In Section .1 from Equations (67) to (79), the full optimization formulation for the Multi-Period Optimal Power Flow (MPOPF) problem using the LinDistFlow model is presented.

## .1 Full MPOPF Formulation with LinDistFlow

**Sets:**

- $\mathbb{N}$ : Set of all buses, with substation bus  $j_1 \in \mathbb{N}$
- $\mathbb{N} \setminus \{j_1\}$ : Set of non-substation buses
- $\mathbb{L}$ : Set of all branches (directed edges)
- $\mathbb{L}_1$ : Set of branches directly connected to substation bus  $j_1$
- $\mathbb{L} \setminus \mathbb{L}_1$ : Set of branches not connected to substation
- $\mathbb{B}$ : Set of buses with battery storage
- $\mathbb{D}$ : Set of buses with distributed energy resources (DERs)
- $\mathbb{T}$ : Set of time periods  $\{1, 2, \dots, T\}$

**Objective Function:**

$$\min \sum_{t \in \mathbb{T}} C^t P_{\text{Subs}}^t \Delta t + \sum_{t \in \mathbb{T}} \sum_{j \in \mathbb{B}} C_B (P_{B_j}^t)^2 \Delta t \quad (67)$$

**Subject to:**

*Power Balance at Substation Bus ( $j = j_1$ ):*

$$P_{\text{Subs}}^t - \sum_{(j_1, k) \in \mathbb{L}_1} P_{j_1 k}^t = 0, \quad \forall t \in \mathbb{T} \quad (68)$$

$$Q_{\text{Subs}}^t - \sum_{(j_1, k) \in \mathbb{L}_1} Q_{j_1 k}^t = 0, \quad \forall t \in \mathbb{T} \quad (69)$$

*Power Balance at Non-Substation Buses ( $j \in \mathbb{N} \setminus \{j_1\}$ ):*

$$\sum_{(j, k) \in \mathbb{L}} P_{jk}^t - \sum_{(i, j) \in \mathbb{L}} P_{ij}^t = P_{B_j}^t + p_{D_j}^t - p_{L_j}^t, \quad \forall j \in \mathbb{N}, \forall t \in \mathbb{T} \quad (70)$$

$$\sum_{(j, k) \in \mathbb{L}} Q_{jk}^t - \sum_{(i, j) \in \mathbb{L}} Q_{ij}^t = q_{D_j}^t - q_{L_j}^t, \quad \forall j \in \mathbb{N}, \forall t \in \mathbb{T} \quad (71)$$

*Voltage Drop (LinDistFlow KVL):*

$$v_j^t = v_i^t - 2(r_{ij}P_{ij}^t + x_{ij}Q_{ij}^t), \quad \forall(i, j) \in \mathbb{L}, \forall t \in \mathbb{T} \quad (72)$$

*Substation Voltage:*

$$v_{j1}^t = v_{\text{nom}}^2, \quad \forall t \in \mathbb{T} \quad (73)$$

*Voltage Limits:*

$$(v_{\min})^2 \leq v_j^t \leq (v_{\max})^2, \quad \forall j \in \mathbb{N}, \forall t \in \mathbb{T} \quad (74)$$

*Battery State of Charge:*

$$B_j^t = B_j^{t-1} - P_{B_j}^t \Delta t, \quad \forall j \in \mathbb{B}, \forall t \in \mathbb{T} \setminus \{1\} \quad (75)$$

$$B_j^1 = B_{j,0}, \quad \forall j \in \mathbb{B} \quad (76)$$

*Battery Constraints:*

$$\text{SOC}_{\min} B_{R_j} \leq B_j^t \leq \text{SOC}_{\max} B_{R_j}, \quad \forall j \in \mathbb{B}, \forall t \in \mathbb{T} \quad (77)$$

$$-P_{B_{R_j}} \leq P_{B_j}^t \leq P_{B_{R_j}}, \quad \forall j \in \mathbb{B}, \forall t \in \mathbb{T} \quad (78)$$

*PV Reactive Power Limits:*

$$-\sqrt{S_{D_{R_j}}^2 - (p_{D_j}^t)^2} \leq q_{D_j}^t \leq \sqrt{S_{D_{R_j}}^2 - (p_{D_j}^t)^2}, \quad \forall j \in \mathbb{D}, \forall t \in \mathbb{T} \quad (79)$$

### Variables:

- $P_{\text{Subs}}^t, Q_{\text{Subs}}^t$ : Substation real and reactive power at time  $t$
- $P_{ij}^t, Q_{ij}^t$ : Sending-end real and reactive power flow on branch  $(i, j)$  at time  $t$
- $v_j^t$ : Squared voltage magnitude at bus  $j$  at time  $t$
- $P_{B_j}^t$ : Battery power at bus  $j$  at time  $t$  (positive = discharging)
- $B_j^t$ : Battery state of charge at bus  $j$  at time  $t$
- $q_{D_j}^t$ : PV reactive power injection at bus  $j$  at time  $t$

### Parameters:

- $C^t$ : Energy cost at time  $t$  (\$/kWh)
- $C_B$ : Battery degradation cost coefficient
- $\Delta t$ : Time step duration

- $r_{ij}, x_{ij}$ : Branch resistance and reactance
- $p_{L_j}^t, q_{L_j}^t$ : Load real and reactive power at bus  $j$  at time  $t$
- $p_{D_j}^t$ : PV real power generation at bus  $j$  at time  $t$
- $B_{R_j}, P_{B_{R_j}}$ : Battery energy and power capacity at bus  $j$
- $S_{D_{R_j}}$ : PV apparent power capacity at bus  $j$

## References

- [1] A. R. Jha, S. Paul, and A. Dubey, “Analyzing the Performance of Linear and Nonlinear Multi - Period Optimal Power Flow Models for Active Distribution Networks,” *Published in: 2025 IEEE North-East India International Energy Conversion Conference and Exhibition (NE-IECCE)*, pp. 04–06.
- [2] N. Nazir, P. Racherla, and M. Almassalkhi, “Optimal multi-period dispatch of distributed energy resources in unbalanced distribution feeders,” *arXiv*, Jun. 2019.
- [3] A. Agarwal and L. Pileggi, “Large Scale Multi-Period Optimal Power Flow With Energy Storage Systems Using Differential Dynamic Programming,” *IEEE Trans. Power Syst.*, vol. 37, no. 3, pp. 1750–1759, Sep. 2021.
- [4] M. Farivar and S. H. Low, “Branch Flow Model: Relaxations and Convexification—Part I,” *IEEE Trans. Power Syst.*, vol. 28, no. 3, pp. 2554–2564, Apr. 2013.
- [5] A. Gabash and P. Li, “Active-reactive optimal power flow in distribution networks with embedded generation and battery storage,” *IEEE Trans. Power Syst.*, vol. 27, no. 4, pp. 2026–2035, Nov. 2012.
- [6] N. Nazir and M. Almassalkhi, “Receding-Horizon Optimization of Unbalanced Distribution Systems with Time-Scale Separation for Discrete and Continuous Control Devices,” *2018 Power Systems Computation Conference (PSCC)*, pp. 1–7, Jun. 2018.
- [7] L. Gan, U. Topcu, and S. H. Low, “Convex Relaxation of Optimal Power Flow Part I: Formulations and Equivalence,” in *IEEE Transactions on Power Systems*, 2015, vol. 30, no. 1, pp. 290–301.
- [8] A. R. Jha, S. Paul, and A. Dubey, “Spatially Distributed Multi-Period Optimal Power Flow with Battery Energy Storage Systems,” *Published in: 2024 56th North American Power Symposium (NAPS)*, pp. 13–15.
- [9] G. Valverde, E. M. G. de Oliveira, A. M. V. de Lara, J. R. S. Peres, and N. Favilla, “Multiperiod optimum power flow for active distribution networks incorporating distributed generation and energy storage systems,” *IEEE Transactions on Industry Applications*, 2021. [Online]. Available: <https://ieeexplore.ieee.org/document/9502092/>
- [10] A. G. B. et al., “Large scale multi-period optimal power flow with energy storage,” *IEEE Transactions on Power Systems*, 2021. [Online]. Available: <https://ieeexplore.ieee.org/document/9549701/>
- [11] ———, “Large scale multi-period optimal power flow with energy storage,” *IEEE Transactions on Power Systems*, 2021. [Online]. Available: <https://ieeexplore.ieee.org/document/9549701/>

- [12] C. Wu, W. Gu, S. Zhou, and X. Chen, “Coordinated optimal power flow for integrated active distribution network and virtual power plants using decentralized algorithm,” *IEEE Trans. Power Syst.*, vol. 36, no. 4, pp. 3541–3551, Jul. 2021.
- [13] M. Farivar and S. H. Low, “Branch flow model: Relaxations and convexification—part i,” *IEEE Trans. Power Syst.*, vol. 28, no. 3, pp. 2554–2564, 2013.
- [14] A. Safdarian, M. Fotuhi-Firuzabad, and M. Lehtonen, “Benefits of demand response on operation of distribution networks: A case study,” *IEEE Syst. J.*, vol. 10, no. 1, pp. 189–197, 2016.
- [15] A. R. Jha, S. Paul, and A. Dubey, “Spatially distributed multi-period optimal power flow with battery energy storage systems,” in *2024 56th North American Power Symposium (NAPS)*, 2024, pp. 1–6.
- [16] P. Li, W. Wu, X. Wang, and B. Xu, “A data-driven linear optimal power flow model for distribution networks,” *IEEE Trans. Power Syst.*, vol. 38, no. 1, pp. 956–959, 2023.
- [17] C. Lei, S. Bu, Q. Chen, Q. Wang, Q. Wang, and D. Srinivasan, “Decentralized optimal power flow for multi-agent active distribution networks: A differentially private consensus admm algorithm,” *IEEE Trans. Smart Grid*, vol. 15, no. 6, pp. 6175–6178, 2024.
- [18] S. Paul and N. P. Padhy, “Real-time advanced energy-efficient management of an active radial distribution network,” *IEEE Syst. J.*, vol. 16, no. 3, pp. 3602–3612, Sept. 2022.
- [19] T. Yang, Y. Guo, L. Deng, H. Sun, and W. Wu, “A linear branch flow model for radial distribution networks and its application to reactive power optimization and network reconfiguration,” *IEEE Trans. Smart Grid*, vol. 12, no. 3, pp. 2027–2036, 2021.
- [20] S. R. Vaishya, A. R. Abhyankar, and P. Kumar, “A novel loss sensitivity based linearized opf and lmp calculations for active balanced distribution networks,” *IEEE Syst. J.*, vol. 17, no. 1, pp. 1340–1351, 2023.
- [21] N. Nazir and M. Almassalkhi, “Guaranteeing a Physically Realizable Battery Dispatch Without Charge-Discharge Complementarity Constraints,” *IEEE Trans. Smart Grid*, vol. 14, no. 3, pp. 2473–2476, Sep. 2021.
- [22] H. Ahmadi and J. R. Martí, “Linear Current Flow Equations With Application to Distribution Systems Reconfiguration,” *IEEE Trans. Power Syst.*, vol. 30, no. 4, pp. 2073–2080, Oct. 2014.
- [23] M. Lubin, O. Dowson, J. Dias Garcia, J. Huchette, B. Legat, and J. P. Vielma, “JuMP 1.0: Recent improvements to a modeling language for mathematical optimization,” *Mathematical Programming Computation*, vol. 15, p. 581–589, 2023.
- [24] A. Wächter and L. T. Biegler, “On the implementation of an interior-point filter line-search algorithm for large-scale nonlinear programming,” *Math. Program.*, vol. 106, no. 1, pp. 25–57, Mar. 2006.

- [25] “OpenDSSDirect.jl,” Mar. 2025, [Online; accessed 9. Mar. 2025]. [Online]. Available: <https://github.com/dss-extensions/OpenDSSDirect.jl>
- [26] “MultiPeriod-DistOPF-Benchmark,” Jul. 2024, [Online; accessed 15. Jul. 2024]. [Online]. Available: <https://github.com/Realife-Brahmin/MultiPeriod-DistOPF-Benchmark>
- [27] T. Gangwar, N. P. Padhy, and P. Jena, “Storage allocation in active distribution networks considering life cycle and uncertainty,” *IEEE Trans. Ind. Inform.*, vol. 19, no. 1, pp. 339–350, Jan. 2023.
- [28] W. Wei, J. Wang, and L. Wu, “Distribution optimal power flow with real-time price elasticity,” *IEEE Trans. Power Syst.*, vol. 33, no. 1, pp. 1097–1098, Jan. 2018.
- [29] M. M.-U.-T. Chowdhury, B. D. Biswas, and S. Kamalasadan, “Second-order cone programming (socp) model for three phase optimal power flow (opf) in active distribution networks,” *IEEE Trans. Smart Grid*, vol. 14, no. 5, pp. 3732–3743, 2023.
- [30] Z. Guo, W. Wei, L. Chen, Z. Dong, and S. Mei, “Parametric distribution optimal power flow with variable renewable generation,” *IEEE Trans. Power Syst.*, vol. 37, no. 3, pp. 1831–1841, May 2022.
- [31] H. Yuan, F. Li, Y. Wei, and J. Zhu, “Novel linearized power flow and linearized opf models for active distribution networks with application in distribution lmp,” *IEEE Trans. Smart Grid*, vol. 9, no. 1, pp. 438–448, Jan. 2018.
- [32] A. R. Di Fazio, C. Risi, M. Russo, and M. De Santis, “Decentralized voltage optimization based on the auxiliary problem principle in distribution networks with ders,” *Appl. Sci.*, vol. 11, no. 4509, pp. 1–24, 2021.
- [33] W. Zheng, W. Wu, B. Zhang, H. Sun, and Y. Liu, “A fully distributed reactive power optimization and control method for active distribution networks,” *IEEE Trans. Smart Grid*, vol. 7, no. 2, pp. 1021–1033, Mar. 2016.
- [34] P. Wang, Q. Wu, S. Huang, C. Li, and B. Zhou, “Admm-based distributed active and reactive power control for regional ac power grid with wind farms,” *J. Modern Power Syst. Clean Energy*, vol. 10, no. 3, pp. 588–596, May 2022.
- [35] B. D. Biswas, M. S. Hasan, and S. Kamalasadan, “Decentralized distributed convex optimal power flow model for power distribution system based on alternating direction method of multipliers,” *IEEE Trans. Ind. Appl.*, vol. 59, no. 1, pp. 627–640, Jan.-Feb. 2023.
- [36] S. Paul, B. Ganguly, and S. Chatterjee, “Nesterov-type accelerated admm (n-admm) with adaptive penalty for three-phase distributed opf under non-ideal data transfer scenarios,” in *2023 IEEE 3rd International Conference on Smart Technologies for Power, Energy and Control (STPEC)*, 2023, pp. 1–6.

- [37] R. Sadnan and A. Dubey, “Distributed optimization using reduced network equivalents for radial power distribution systems,” *IEEE Trans. Power Syst.*, vol. 36, no. 4, pp. 3645–3656, Jul. 2021.
- [38] M. Alizadeh and V. Capitanescu, “Stochastic security-constrained multi-period optimal power flow,” *Electric Power Systems Research*, vol. 189, p. 106660, 2020.
- [39] M. Usman and V. Capitanescu, “Multi-period ac optimal power flow: Formulations and solution methods,” *IEEE Transactions on Power Systems*, vol. 32, no. 4, pp. 3268–3277, 2017.
- [40] A. R. Aghdam and M. Shahidehpour, “Optimal battery scheduling for renewable integration using model predictive control,” *IEEE Transactions on Sustainable Energy*, vol. 10, no. 1, pp. 211–220, 2019.
- [41] X. Zhang, X. Yuan, and J. Zhang, “A robust bi-level multi-period optimal dispatch method for distribution networks with ders,” *IEEE Transactions on Power Systems*, vol. 36, no. 3, pp. 2306–2316, 2021.
- [42] “ADMM,” Oct. 2025, [Online; accessed 28. Oct. 2025]. [Online]. Available: <https://stanford.edu/~boyd/admm.html>
- [43] “Index of /~ryantibs/convexopt-F16/lectures,” Oct. 2025, [Online; accessed 28. Oct. 2025]. [Online]. Available: <https://www.stat.cmu.edu/~ryantibs/convexopt-F16/lectures>
- [44] M. E. Baran and F. F. Wu, “Optimal capacitor placement on radial distribution systems,” *IEEE Transactions on Power Delivery*, vol. 4, no. 1, pp. 725–734, 1989.